Ore Geology Reviews 118 (2020) 103352

Contents lists available at ScienceDirect

Ore Geology Reviews

journal homepage: www.elsevier.com/locate/oregeorev

PGE mineralization in andesite explosive breccias associated with the poperechny iron-manganese deposit (Lesser Khingan, Far East Russia): Whole-rock geochemical, ^{190}Pt-^{4}He isotopic, and mineralogical evidence

N.V. Berdnikov[a], V.G. Nevstruev[a], P.K. Kepezhinskas[b,*], A.G. Mochalov[c], O.V. Yakubovich[c,d]

[a] Kosygin Institute of Tectonics and Geophysics, Khabarovsk, Russia
[b] PNK GeoScience, Tampa, FL, USA
[c] Institute of Precambrian Geology and Geochronology, St. Petersburg, Russia
[d] Saint-Petersburg University, Saint-Petersburg, Russia

ARTICLE INFO

Keywords:
Platinum-group minerals
Explosivebreccia
Alaskan-type complexes
Slab windows

ABSTRACT

We report in this paper an unusual occurrence of platinum-group minerals in evolved explosive breccia associated with the Poperechny iron-manganese deposit (Lesser Khingan Range, Far East Russia). PGMs in andesite breccia are represented by Fe-Pt solid solutions (85%) and PGM (mostly Os-Ir-Ru) solid solutions, sulfides and sulfarsenides (15%). Textural and compositional variations in PGM assemblages suggest that Pt-Fe and Os-Ir-Ru solid solutions, as well as erlichmanite-laurite series sulfides were formed during high-temperature fractionation of mantle-derived mafic parental melt (similar to Alaskan-type complexes) and were entrained in the evolved andesitic melt during its emplacement in the crust. Pd-Pt plumbostannide and copper-gold solid solutions reflect late magmatic re-crystallization and metasomatism. Early Cretaceous (~125 Ma) age of ferroplatinum in the explosive breccia suggests that PGM-bearing ultramafic material could have been sampled during regional slab-window tectonics related to the Late Mesozoic subduction of Izanagi plate along southern margin of the North Asian continent.

1. Introduction

Platinum-group minerals (PGM) are typically associated with cratonic layered intrusions (Maier, 2005; Naldrett et al., 2009; Barnes et al., 2015), Ni-Cu sulfides ores in continental rifts (Maier and Groves, 2011), ophiolitic chromitites (Ahmed and Arai, 2003; Prichard and Brough, 2009), Alaskan-type ultramafic complexes (Kepezhinskas and Defant, 2001; Zaccarini et al., 2018) and modern placer deposits derived from various ultramafic-mafic magmatic rocks (Tolstykh et al., 2002; Walker et al., 2005). These PGM assemblages crystallized from mafic (boninite, Mg-basalt) or ultramafic (picrite) magma under upper mantle or crustal conditions (Lambert et al., 1989; Woodland et al., 2002; Kepezhinskas et al., 2019). PGM occurrences outside the ultramafic-mafic realm are quite rare and are reported from arc-related differentiated lavas in back-arc basins (Park et al., 2013), late-stage dioritic and granophyric dikes in continental layered intrusions (Hanley et al., 2005; Pentek et al., 2013), as well as epigenetic gold-platinum-group mineralization within complex hydrothermal-igneous-sedimentary environments (Moroni et al., 2001; Sener et al., 2002). In this case, distribution of platinum-group minerals appears to be controlled by hydrothermal reactions, sedimentary environments and/or intermediate to felsic (frequently explosive) volcanism.

In this paper we present whole-rock geochemical, isotopic and mineralogical evidence for platinum-group elements mineralization in andesite explosive breccia structurally associated with iron-manganese deposit hosted in Neoproterozoic carbonates in Lesser Khingan Range of Far East Russia. Because these evolved rocks exhibit (Berdnikov et al., 2017) high concentrations of platinum group elements (up to 11.3 ppm of total PGEs) and gold (up to 2.35 ppm), petrologic, geochemical and genetic aspects of PGM occurrences associated with intermediate to felsic magmatism deserve special attention and serve as primary focus of the current study. We attempt in this paper to 1) document platinum-group mineral assemblages deposited by fluid-rich, intermediate volcanism, 2) determine age of PGE crystallization using novel ^{140}Pt-^{4}He isotope method and 3) discuss potential role of subduction-related tectonic processes in formation of some PGE mineralization associated with fluid-rich andesitic magmas.

* Corresponding author.
E-mail address: pavel_k7@yahoo.com (P.K. Kepezhinskas).

https://doi.org/10.1016/j.oregeorev.2020.103352
Received 23 September 2019; Received in revised form 9 January 2020; Accepted 17 January 2020
Available online 23 January 2020

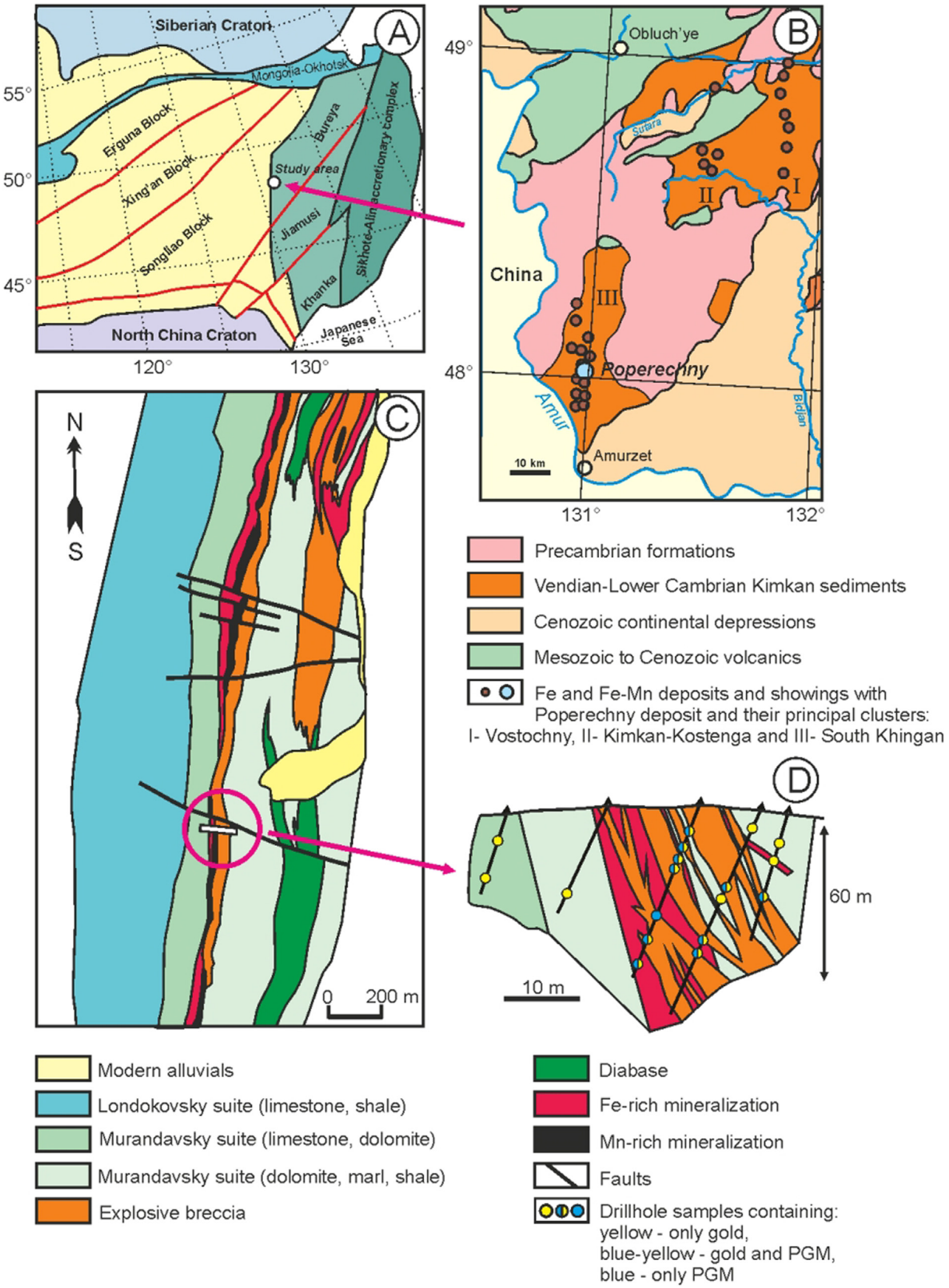

Fig. 1. A – location of the Bureinsky Block and the Lesser Khingan terrane in Eastern Asia (after Yang et al., 2014). B – Schematic tectonic map of the Lesser Khingan terrane (after Berdnikov et al., 2017). C – Simplified geologic map of the Poperechny iron-manganese deposit (after Berdnikov et al., 2017). D - Schematic geologic cross-section through the northern part of the main ore body at the Poperechny deposit showing drill intervals sampled for precious metal mineralization presented in this study.

2. Geologic setting

Lesser Khingan Range forms a part (Bureya block) of the Bureya-Khanka super-terrane (Fig. 1A) composed of the Lesser Khingan Precambrian rock formations tectonically overprinted with Neoproterozoic-Early Cambrian Kimkan pericratonic trough and re-mobilized at the later stage within the Cretaceous Khingan-Olonoy magmatic belt of possible subduction-related origin (Didenko et al., 2010; Liu et al., 2017; Luan et al., 2017).

Lesser Khingan terrane (Fig. 1B) includes ten structural-compositional units (complexes): 1) Precambrian plutonic and metamorphic (low-grade metavolcanics and metasediments intruded by various granites); 2) Paleo-Proterozoic marbles, graphite-rich schists and quartzites; 3) Late Riphean-Early Cambrian carbonates and clastic metasediments; 4) Ordovician gabbros and granites; 5) Middle to Late Carboniferous gabbros, granodiorites and granites; 6) Permian-Triassic monzonites and subalkaline leucogranites; 7) Early Cretaceous clastic sediments, calc-alkaline volcanics (basalts, basaltic andesites, dacites, rhyolites) intruded by gabbro-granodiorite-granite (comagmatic?) intrusive series; 8) Late Cretaceous calc-alkaline volcanics and associated granitoids; 9) Miocene molasses and associated alkaline basalts and dolerites and 10) Pliocene-Quaternary molasses and modern sediments.

Precambrian rocks (Fig. 1B) are folded into inclining linear fold pattern and include mafic metavolcanics and metasediments metamorphosed in epidote amphibolite to amphibolite-facies conditions. Amphibolites are frequently migmatized and contain tectonic boudines of garnet peridotites. Precambrian package is intruded by gneissic gabbros and tonalites. Paleoproterozoic units include marble, graphite schist and quartzite impregnated with granodiorite-tonalite-granite series. These geologic structures were re-activated in Riphean-Early Cambrian time and filled with carbonates, terrigeneous sediments (carbonaceous sandstone and mudstone) and greenschist-facies cherts.

Intense sedimentation, folding and metamorphism at the Precambrian-Phanerozoic transition in the Lesser Khingan terrane was followed by the large-scale Paleozoic gabbro-granodiorite-granite magmatism with predominant high-K calc-alkaline and shoshonitic chemistry (Berdnikov et al., 2017). During Mesozoic, Lesser Khingan was involved in development of multiple subduction zones and active continental margins collectively related to the closure of the Mongol-Okhotsk Ocean and marked by calc-alkaline to shoshonitic volcanic series and associated granitoids (Didenko et al., 2010; Khanchuk et al., 2015). Collision processes along the contact zone between the Siberian craton to the north and North China craton to the south (Fig. 1A) resulted in formation of structurally complex thrust systems which, along with the later-stage normal and reverse faulting, dominate modern structure of the Lesser Khingan terrane (Didenko et al., 2010; Khanchuk et al., 2015).

The Lesser Khingan terrane occupies the westernmost part of the Bureya block and essentially represents an ancient accretionary prism metamorphosed in the Early Ordovician (Khanchuk et al., 2013; Khanchuk et al., 2015). Based on isotopic data, the age of protolith formations ranges from 1.2 to 0.5 Ga, while age of regional metamorphism within the Bureya block is dated at around 490 Ma (Sorokin et al., 2010). The iron-manganese mineralization is cropping out within a 40-km wide zone from the Kimkan River in the north to the Amur River in the south (Fig. 1B) and is continuous southwards into China, where it includes Yilan cluster of Fe-Mn showings. All Fe-Mn deposits and mineral showings can be grouped in three principal clusters: Vostochny, Kimkan-Kostenga and South Khingan (Fig. 1B).

The Poperechny iron-manganese deposit is located within the southern part of South Khingan cluster (Fig. 1B). Fe-Mn mineralization is hosted in Late Riphean-Vendian carbonates of the Murandavsky suite (Fig. 1C). Mineralization is displaced laterally with amplitude of several tens of meters by later-stage faults (Fig. 1C). Eastern part of the Poperechny deposit is localized within massive-textured dolomite unit with subordinate siliceous dolomites, carbonaceous shales and phyllites. Western boundary of the Poperechny ore field is associated with black pelitic limestone intercalated with cherty shale and dolomitized sandstone (Fig. 1C).

A narrow (first meters to 15–20 m wide) zone composed of explosive breccia is traced along the eastern side of the deposit (Fig. 1C and D). These breccias, which were originally interpreted as sedimentary rocks, are in direct contact with ore-grade, Fe-Mn mineralization (Berdnikov et al., 2017; Nevstruyev et al., 2018). Based on the exploration drilling (Fig. 1D), explosive breccias form isolated zones and wide veins in both sedimentary country rocks as well as iron-rich and manganese-rich mineralized zones (Berdnikov et al., 2017). Composite zones of sub-volcanic rocks intermingled with ferruginous quartzite and low-grade manganese mineralization have been mapped via drilling in the hanging wall of the main ore body within the northern part of the Poperecnhy Fe-Mn deposit (Fig. 1C). It is important to emphasize here that geologic relationships presented in detail in Fig. 1C and D indicate non-contemporary origin of the iron-manganese mineralization and its host carbonates. We also present in this paper decisive evidence for a later-stage formation of PGM mineralization, specifically in comparison with carbonate-rich lithologies at the Poperechny deposit, which appear to have Late Riphean-Vendian age (Smirnova et al., 2016). The age of iron-manganese ores at Poperechny is currently unknown, which precludes, at least at this point, any inferences into temporal relationships between Fe-Mn and PGM mineralization.

3. Analytical methods

Major element compositions of the bulk rock and ore samples were determined on pressed pellets mixed with lithium metaborate using a S4 Pioneer X-ray fluorescence (XRF) spectrometer. International - LDI-3 (gabbro) and WMG-1a (mineralized gabbro) – as well as Russian – DVB (basaltic andesite), DVA (andesite) and DVD (dacite) – reference standards were used for calibration. Analytical uncertainty for major elements is ± 10%. Trace element abundances of bulk rock samples were measured using an ELAN 9000 ICP-MS after an acid digestion of sample powders. The same set of rock reference standards (LDI-3, WMG-1a, DVB, DVA and DVD) along with Perkin Elmer standard solutions PE# N9300231-9300234 were used to monitor analytical accuracy and precision. The accuracy was ± 5% for the trace elements with abundances of > 20 ppm and ± 10% for elements with abundances of < 20 ppm. The analytical details are as reported in Berdnikov et al. (2017).

Chemical compositions and elemental maps of minerals were obtained using a VEGA 3 LMH TESCAN scanning electron microscope with the Oxford X-Max 80 energy dispersion spectrometer (EDS). The EDS analyses were carried out using various metal and mineral standards (Pt, Ir, Rh, Ru, Pt_3Fe, PtFe, laurite, sperrylite). Individual grains as well as polished sections and rough surfaces of rocks and ores were used for investigation by the SEM. In some cases, platinum-group minerals were studied in several (commonly 3 or 4) parallel cuts with 10 μm steps, or acid etched with HF in order to expose microinclusions of PGE sulfides in platinum grains. All these analytical procedures were carried out at the Khabarovsk Innovative-Analytical Center (KhIAC, Khabarovsk, Russian Federation).

Direct determination of magmatic crystallization ages on isolated platinum grains using ^{190}Pt-^{4}He isotope equilibrium was done following protocols and techniques developed and summarized in Shukolyukov et al. (2012, 2014) and Savatenkov and Mochalov (2013). The ^{190}Pt-^{4}He method of isotope dating is based on high preservation rate of radiogenic helium in platinum minerals (Shukolyukov et al., 2012). Basic foundations of this method were developed using magmatic platinum-group minerals from the unique Konder platinum placer deposits (Nekrasov et al., 2005; Burg et al., 2009), for which co-magmatic origin with PGE mineralization in ultramafic source rocks with available isotopic (Re-Os, Sm-Nd, U-Pb and Rb-Sr methods) ages from the Konder alkaline-ultrabasic intrusion were established beyond any reasonable

doubt (Cabri et al., 1998; Savatenkov and Mochalov, 2013). Individual isoferroplatinum grains from the Konder placers have been dated using $^{190}Pt/^{4}He$ method at 129 ± 6 Ma (Mochalov et al., 2016), which is in excellent agreement with dating Konder PGE mineralization in core dunites using alternative (U-Pb on zircon and baddeleyite, model Re-Os and Sm-Nd, clinopyroxene-derived Sm-Nd) methods of isotope geochronology (Malitch and Thalhammer, 2002; Nekrasov et al., 2005; Malitch et al., 2012; Savatenkov and Mochalov, 2013). Moreover, structural studies combined with $^{190}Pt/^{4}Fe$ isotope dating of platinum from both placers and dunites from the Konder core (central zone) suggest that various degrees of mechanical deformations of platinum and isoferroplatinum grains from Konder placers have no detectable effect on their isotopic ages (Mochalov et al., 2018). In addition, results of ^{190}Pt-^{4}He dating of individual platinum grains from several platinum deposits of the Russian Far East are in good agreement with their ages established using independent isotopic systems, as well as general geologic and structural data (Shukolyukov et al., 2014).

Platinum grains from the Poperechny explosive breccias have been thoroughly investigated using stereoscopic microscope, and all crystals containing inclusions of other PGEs were excluded from the current isotopic study. One or several optically homogeneous grains were then wrapped in tantalum foil with addition of pure copper metal following techniques of Shukolyukov et al. (2012, 2014). At the same time, a reference sample composed only of tantalum foil and pure copper has been prepared. Samples were then loaded into a rhenium cylinder using specially constructed loading docks (Shukolyukov et al., 2012; Mochalov et al., 2016) and were step-heated up to a temperature of approximately 1400 °C. Gases emitted at each heating stage were collected and purified using two SAES non-evaporable getters with selective sorption of H_2, N_2, O_2, H_2O, CO_2 and other gaseous species (Shukolyukov et al., 2014). Helium was ionized using electron impact technique (Shukolyukov et al., 2012; Mochalov et al., 2016). Radiogenic helium was measured using sector mass-spectrometer MSU-G-01-M at the Institute of Precambrian Geology and Geochronology (St. Petersburg, Russian Federation) with spectrometer detection limit of $\sim 5 \times 10^{-12}$ cm^3. Values obtained from tantalum foil/copper runs were systematically below 1×10^{-10} см^3 ^{4}He.

4. Petrography and geochemistry of explosive breccias

Carbonates hosting both explosive volcanic rocks and iron-manganese mineralization are mostly massive, fine- to medium-grained dolomites and limestones of the Murandavsky suite, which locally, primarily along the contacts with igneous rocks, were converted into marble with a coarser grain size distribution in comparison with pre-contact metamorphosed carbonates (Berdnikov et al., 2017). Carbonate slivers among volcanic rocks are usually fractured (possibly due to explosive emplacement of felsic magma) and these post-depositional fractures are filled with coarse-grained (metasomatic?) calcite, quartz, magnetite, hematite and braunite. Carbonates hosting igneous veins are also frequently silicified and sulfidized, commonly together with explosive igneous material.

Explosive rocks from the Poperechny Fe-Mn deposit display clear brecciated texture (Fig. 2C and D) composed of sharp angular fragments of various country-rock units «immersed» in fine-grained, glass-bearing (rarely) matrix (Fig. 2A). Breccia fragments (clasts) typically account for 40–60% of the total rock volume and range in size from 0.1 to 0.3 mm to 5 cm, rarely 10–20 cm. Various carbonates dominate the clast population (Fig. 2d) with subordinate ore fragments as well as porphyroclasts representing previous generations of intermediate to felsic explosive rocks (Fig. 2C). Clasts of both carbonate and igneous composition are commonly replaced with secondary ore minerals (Berdnikov et al., 2017). Matrix of these volcanic breccias frequently displays ignimbritic, «fiamme»-like textures (Fig. 2A and B), containing phenocrysts of quartz and carbonated feldspar. Secondary alteration includes chlorite, serecite, hematite, sulfides, quartz-chlorite and dolomite veinlets, as well as locally intense dolomitization, silicification and pyritization. Igneous veins frequently display cross-cutting relationships with carbonate matrix (Berdnikov et al., 2017). In summary, petrographic and geologic data suggest that explosive breccia emplacement post-dates accumulation of host carbonates of the Upper Riphean-Vendian age (Smirnova et al., 2016).

Possible genetic relationships between andesite breccia and Fe-Mn mineralization are unclear at this point. Petrographic observations suggest presence of fragments of Fe-Mn ore in andesite breccia and veins of andesitic composition in Fe-Mn ore, along with replacement of minerals in andesitic breccia by Fe-Mn oxides and hydroxides. These complex textural relationships might be indicative of Fe-Mn mineralization being a) contemporaneous with andesite volcanism and b) multi-stage in nature. Temporal association between the Fe-Mn and PGM mineralization is rather unclear at this stage, as we failed to observe any textural relationships between the PGM and iron-manganese minerals in thin sections, probably due to the overall small size (microns) of PGM grains and the mode of their recovery (separation by gravitation) from the original rock samples. It is important to emphasize that we did not observe replacement of Fe-Mn phases in the explosive breccia by platinum-group minerals. Existing petrologic information suggests either somewhat earlier formation of PGM assemblages, or general close temporal association between the explosive breccia, Fe-Mn and PGM mineralization.

Major and trace element contents in explosive breccias associated with Poperechny iron-manganese deposit are listed in Table 1. Their composition varies from basaltic (44.89–50.68 wt% SiO_2 and 7.02–8.20 wt% MgO; Table 1) to dacitic (64.15 wt% SiO_2 and 4.37 wt% MgO; Table 1) with relatively low Al_2O_3, CaO and Na_2O contents (10.80–14.28 wt%, 2.05–6.88 wt% with an exception of high-Ca basaltic sample 3–05 with 10.87 wt%; 0.20–2.38 wt% respectively; Table 1). All samples are enriched in K_2O (2.69–3.98 wt%; K_2O/Na_2O = 1.17–17.60; Table 1) and are classified as either shoshonitic or high-K calc-alkaline series. Some volcanic breccias display elevated MgO contents in the basaltic andesite (samples 3–13, 4–14 and 4–31 with 5.93, 5.88 and 6.06 wt% MgO, respectively; Table 1) and andesite (samples 4–01, 4–10, 4–13 and 4–17 with 5.94, 5.33, 4.99 and 6.22 wt % MgO, respectively; Table 1) compositional range, similar to some

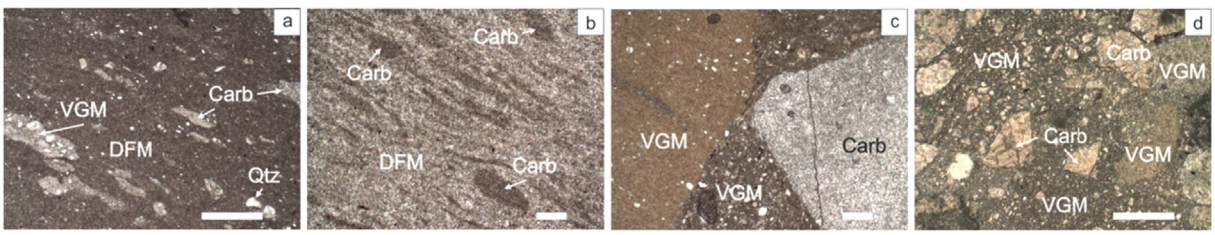

Fig. 2. Typical textures of felsic explosive breccias associated with the Poperecheny iron-manganese deposit: a – felsic explosive breccia; b – carbonated (dolomitized) felsic explosive breccia; c – various types of felsic explosive material juxtaposed on a microscale; d – tuffaceous texture in felsic breccia. Carb – carbonates, Qtz – quartz, DFM – dolomitized felsic matrix, VGM – various generations of felsic explosive material juxtaposed on a micro-scale. Horizontal scale bar for all microphotographs is 40 μm.

Table 1
Major (wt.%) and trace (ppm) element concentrations in differentiated explosive breccias from the Poperechny Fe-Mn deposit.

Sample	2–03	2–04	3–05	3–06	3–10	3–13	4–01	4–08	4–10	4–13	4–14	4–17	4–31
SiO_2	57,08	58,04	44,89	50,68	57,91	53,52	56,61	64,15	58,92	58,54	54,78	56,66	53,30
TiO_2	0,92	0,87	0,82	0,81	0,96	0,90	0,66	0,73	0,74	0,71	0,72	0,67	0,88
Al_2O_3	14,28	13,06	10,95	11,37	13,28	12,47	10,80	13,23	11,99	12,38	10,82	10,95	12,75
Fe_2O_3	7,76	9,24	5,71	9,02	7,65	5,06	4,83	3,84	6,26	5,87	5,41	5,84	4,52
MnO	0,05	0,10	0,28	0,18	0,18	0,58	0,09	0,05	0,07	0,07	0,09	0,14	0,61
CaO	3,09	3,59	10,87	6,88	2,05	6,00	6,30	4,63	4,94	4,93	6,78	6,72	6,49
MgO	3,12	3,33	8,20	7,02	4,62	5,93	5,94	4,37	5,33	4,99	5,88	6,22	6,06
Na_2O	0,24	0,22	0,66	1,08	2,38	1,08	0,21	0,20	0,21	0,22	0,22	0,29	0,68
K_2O	3,98	3,61	2,94	2,34	2,78	3,62	2,69	3,52	3,03	3,19	2,84	2,71	3,87
P_2O_5	0,10	0,11	0,08	0,08	0,12	0,11	0,13	0,14	0,14	0,14	0,12	0,14	0,11
Sc	14,60	17,83	12,90	15,65	16,08	12,90	10,23	10,96	11,75	12,08	10,37	10,81	16,99
V	147,26	152,13	54,70	62,58	75,67	87,03	84,41	177,39	199,19	147,71	219,50	162,93	91,84
Cr	96,91	103,83	31,52	34,57	43,32	41,81	47,82	88,93	104,59	85,18	101,98	88,85	52,74
Co	29,43	33,86	10,15	8,93	12,57	53,49	10,65	9,59	13,09	13,30	10,10	29,90	40,28
Ni	72,13	126,07	108,74	106,73	276,33	509,14	65,87	46,20	72,75	98,95	82,73	158,40	558,38
Cu	31,56	40,82	35,17	49,24	45,69	71,79	39,52	47,29	42,93	68,40	36,30	47,32	50,39
Zn	133,61	118,55	51,45	73,30	103,55	117,64	128,95	64,48	108,98	166,07	63,91	103,94	108,00
Ga	18,23	15,96	13,94	15,24	19,58	17,07	14,98	14,62	15,74	14,95	12,56	14,13	18,28
Rb	131,42	123,38	108,44	89,67	100,08	128,82	106,90	126,59	116,47	118,94	103,68	102,26	147,77
Sr	38,18	34,82	74,26	56,54	50,62	65,64	62,22	62,48	75,12	78,06	81,65	82,70	81,14
Y	16,00	19,47	16,01	14,85	14,31	15,78	16,75	15,10	16,91	16,07	13,54	16,73	16,18
Zr	120,01	89,99	64,94	61,64	74,47	77,74	78,27	69,21	82,19	72,91	64,10	88,31	71,67
Nb	6,49	1,53	2,57	2,10	4,82	3,56	2,63	3,28	2,03	1,57	3,14	3,20	2,52
Ag	1,17	–	0,15	0,29	0,65	1,27	–	1,36	0,62	0,58	0,35	0,55	0,72
Sn	2,57	2,00	2,06	1,99	2,80	2,62	2,10	2,36	1,87	2,22	1,80	1,75	2,72
Cs	5,14	5,00	4,92	4,17	4,49	6,26	5,49	7,28	7,29	6,66	6,98	6,41	8,47
Ba	1380,40	1066,90	658,19	557,71	1350,92	1816,44	452,74	555,10	524,67	505,49	398,81	464,00	1866,70
La	16,72	15,21	24,39	21,43	33,29	27,60	24,72	23,46	25,38	19,95	21,58	23,74	25,71
Ce	39,65	37,23	52,24	48,44	69,73	58,74	57,32	50,09	54,49	43,36	46,24	51,09	56,46
Pr	4,46	4,51	5,94	5,46	7,63	6,38	6,17	5,66	6,24	5,06	5,24	5,76	6,12
Nd	20,09	21,37	24,30	23,56	31,02	25,83	26,36	24,16	26,15	22,09	21,77	24,63	25,37
Sm	4,87	5,55	4,86	5,02	6,11	5,02	5,18	4,72	5,11	4,65	4,13	4,79	5,07
Eu	1,04	1,30	0,90	0,91	0,99	0,88	0,95	0,93	1,01	0,93	0,83	0,96	0,90
Gd	5,30	6,20	4,82	4,93	5,75	4,88	5,17	4,56	5,02	4,70	4,09	4,65	5,26
Tb	0,66	0,82	0,61	0,63	0,65	0,60	0,60	0,52	0,58	0,56	0,48	0,55	0,64
Dy	3,99	4,70	3,62	3,63	3,47	3,43	3,41	2,95	3,33	3,23	2,68	3,16	3,55
Ho	0,72	0,84	0,66	0,64	0,59	0,62	0,62	0,55	0,62	0,60	0,49	0,60	0,62
Er	2,42	2,60	2,00	1,99	1,84	1,92	1,97	1,76	1,96	1,93	1,59	1,93	1,90
Tm	0,33	0,37	0,26	0,26	0,24	0,25	0,26	0,25	0,27	0,26	0,22	0,27	0,24
Yb	2,39	2,63	1,85	1,90	1,70	1,75	1,90	1,78	1,95	1,95	1,60	1,98	1,69
Lu	0,33	0,37	0,26	0,27	0,23	0,25	0,26	0,26	0,28	0,28	0,23	0,29	0,23
Hf	3,74	2,78	1,80	1,69	2,10	2,28	2,13	2,00	2,28	2,06	1,79	2,34	1,84
Ta	0,47	0,12	0,23	0,19	0,40	0,31	0,24	0,24	0,19	0,17	0,52	0,32	0,30
Pb	4,17	8,74	10,42	6,59	4,54	10,67	5,26	5,31	7,76	10,80	3,87	14,18	3,81
Th	9,77	7,17	6,89	6,89	8,31	8,30	6,64	6,58	7,13	7,05	5,84	6,39	7,86
U	1,77	1,67	0,52	0,52	0,64	0,84	1,14	1,46	1,65	1,73	1,25	1,90	0,59
Corg	6,34	6,21	1,82	1,98	0,46	1,02	1,95	2,74	2,78	2,9	2,64	2,11	0,99
K_2O/Na_2O	16,60	16,40	4,46	2,17	1,17	3,35	12,81	17,60	14,43	14,50	12,91	9,35	5,69
Ba/La	82,56	70,15	26,99	26,03	40,58	65,81	18,31	23,66	20,69	25,34	18,50	19,55	72,61
Ba/Nb	212,7	697,3	256,1	265,6	280,3	510,2	172,1	169,2	258,5	322,0	127,0	145,0	740,8
Rb/Y	8,20	6,34	6,77	6,04	7,00	8,16	6,38	8,38	6,89	7,40	7,66	6,11	9,13
La/Nb	2,58	9,94	9,49	10,21	6,91	7,75	9,40	7,15	12,50	12,70	6,87	7,42	10,20
Zr/Sm	24,64	16,21	13,36	12,28	12,19	15,49	15,11	14,66	16,08	15,68	15,52	18,44	14,14
La/Ta	35,58	126,75	106,04	83,23	89,00	89,00	103,00	97,75	133,58	117,35	41,50	74,19	85,70

All analyzed samples are characterized by the least alteration, with an exception of sample 3–06 (weak dolomitization) and sample 4–17 (weak Fe-Mn mineralization). Only samples with minimal amounts of various clasts were selected for major and trace element determinations. Fig. 3

primitive high-MgO andesites in island arc settings (Wood and Turner, 2009). All explosive breccias, with an exception of sample 3–05 (CaO = 10.87 wt%; table 1), exhibit low CaO contents of 2.05–6.88 wt % (Table 1).

Evolved rocks from the Poperechny deposit have low Cr (31–126 ppm) and Co (9–29 ppm) contents, while several basaltic andesites and andesites display unusually high Ni concentrations (276–558 ppm) typical of primary, mantle-derived mafic magmas (Sato, 1977; Yao et al., 2018). All igneous samples exhibit high concentrations of large-ion lithophile elements (LILE), such as Cs, Rb and, especially, Ba (398–1866 ppm, in several samples – 1066–1886 ppm; Table 1) and low high-field strength element (HFSE) contents (Nb, Ta, Hf, Zr, Y) coupled with elevated LILE/HFSE ratios, such as Ba/Nb (127–740) and Rb/Y (6.0–8.4), as well as LILE/LREE ratios, such as Ba/La (18–83) and LREE/HFSE ratios, such as La/Ta (35–134) and La/Nb (2.6–12.7). These trace element ratios suggest broad similarity with various subduction-related magmas (Perfit et al., 1980; Hawkesworth et al., 1993; Kepezhinskas et al., 2020).

Primitive mantle-normalized trace element patterns for explosive breccia samples from the Poperechny iron-manganese deposit display clear HFSE (especially, Nb and Ta) depletions accompanied by LILE and LREE enrichments, which are typical of island-arc magmas (Woodhead et al., 1993; Thirlwall et al., 1994). Some samples are also enriched in lead (Table 1), possible reflecting addition of slab-derived fluid to a depleted mantle wedge source. This is also consistent with chondrite-normalized distributions of rare earth elements in Poperechny igneous samples, which display variable enrichment of light (La to Nd) rare earth elements in respect to heavy rare earths (Table 1).

Table 2
Inventory of platinum-group minerals (PGMs) and gold identified in explosive breccia and Fe-Mn ores (Poperechny deposit), based on SEM/EDX data of individual grains.

PGMs	Total number of grains identified in this study	Host lithologies
Platinum minerals	660	Explosive breccia and Fe-Mn ore
Os-Ir-Ru solid solutions	20	Explosive breccia and Fe-Mn ore
Platinum-group metal sulfides and sulfarsenides	100	Explosive breccia and Fe-Mn ore
Sub-Total for PGMs:	780	
Free (native) gold	270	Explosive breccia, Fe-Mn ore and host carbonates

5. Platinum-group element mineralization

Platinum-group minerals have been recovered from the core material drilled within the Poperechny deposit during earlier exploration. All drill cores were crushed and separated using standard gravitational separation procedures followed by ultrasonic cleaning (Berdnikov et al., 2017; Nevstruyev et al., 2018). Heavy mineral concentrate was manually picked and examined with stereomicroscope. Multiple grains and intergrowths of platinum-group minerals as well as native gold have been recovered from explosive breccia material and Fe-Mn ores and carbonates (Table 2). Bulk core from which precious metals and minerals were recovered yielded total PGE (sum of Pt, Pd, Ir, Ru and Rh) grades ranging from 0.37 to 11.3 ppm and Au grades of 0.18–2.35 ppm (Berdnikov et al., 2017). Most of the precious metal grains are under 0.1 mm in size, while 20% of all recovered grains are 0.1 to 0.25 mm in size. Only one grain of ~0.5 mm (measured in single dimension) has been recovered from the Poperechny drill core (Berdnikov et al., 2017).

Platinum group minerals dominate the heavy mineral population recovered from the explosive breccia and associated iron-manganese mineralization; they were not detected in host carbonate rocks (Table 2).

No significant correlation between presence of PGMs in studied samples and their relative position within the drill core has been established in this study (Table 3; Berdnikov et al., 2017).

Platinum-iron solid solutions in explosive breccia form euhedral to subhedral cubic and octahedral, variably resorbed grains and aggregates (Fig. 3A–D). The Pt-Fe mineral population is dominated by irregular grains with extensive surface dissolution (Fig. 3B) and surface etching (Fig. 3C) features, while well-formed, predominantly cubic crystals (Fig. 3A) are rather rare. Several complex grains composed of isoferroplatinum and Mg-rich (forsteritic) olivine have been also identified (Fig. 3D), suggesting possible affinity with high-temperature (1200–1400 °C) mineral assemblages (Roeder and Jamieson, 1992), such as Alaskan-type ultramafic complexes (Tolstykh et al., 2002).

Fine platinum particles (5–10 μm in size, Fig. 3E) in association with Fe-Mn minerals in iron-manganese ores appear to be free of any impurities with an exception of some ore-related components (such as Mn; Berdnikov et al., 2017).

All grains of Fe-bearing platinum recovered from explosive breccia in this study are generally classified as isoferroplatinum based on nomenclature of Cabri and Feather (1975). However, Pt/Fe ratio of 3 ± 0.2, characteristic of typical isoferroplatinum alloys (Bowles, 1990), is reported for only 152 grains analyzed in this study, while 3 grains of iron-platinum solid solutions have Pt/Fe ratio of 1 ± 0.2 characteristic of tetraferroplatinum compositions (Cabri and Feather, 1975). Samples of the explosive breccia display wide variations in Pt/Fe ratios in iron-platinum solid solutions indicating that the majority of platinum grains are most probably represented by aggregates with mixed compositions. In the absence of other platinum-group elements, these "mixed" grains altogether are identified as ferroplatinum for the remainder of this manuscript.

Ferroplatinum grains from the explosive breccia also contains iridium (2.69–6.35 at.%; 27 grains), palladium (0.92–5.92 at.%; 75 grains), copper (0.81–7.62 at.%; 328 grains), nickel (0.98–5.90 at.%; 107 grains), tin (0.17–2.44 at.%; 37 grains), rhodium (0.23–5.30 at.%; 4 grains) and osmium (0.89–0.90 at.%; 2 grains). Iridium is typically included in cubic ferroplatinum grains, while palladium forms grains with surface dissolution and etching features, platinum overgrowths on other PGMs and platinum grains associated with free gold in Poperechny breccia. Ferroplatinum grains are compositionally homogeneous and exhibit only weak Fe, Cu and Ir enrichments from core to rim (Fig. 4). In addition, micro-particles of platinum in iron-manganese ores do not display characteristic iron, copper and PGE admixtures (Fig. 3E) typical of ferroplatinum solid solutions in andesite breccia.

Several grains of palladium-bearing ferroplatinum exhibit clear increase in copper concentrations (from 0 to 3–4 atomic %) from core to rim (Fig. 5). Copper increase, in most cases, appears not to be accompanied by similar variations in palladium content.

Four sub-types of platinum solid solutions can be recognized on the basis of additional elements present in their chemical compositions: 1) ferroplatinum, 2) iridium-bearing ferroplatinum, 3) copper-bearing ferroplatinum and 4) palladium-bearing ferroplatinum.

5.1. Ferroplatinum

Ferroplatinum grains from explosive breccia frequently contain multiple inclusions of various platinum-group minerals (Table 3). Sulfoarsenides of Rh, Ir, Ru and Os (Fig. 6B, D and F) are most common and are characterized by Rh enrichment in respect to Ir, Ru and Os,

Table 3
Distribution of platinum group metals in the Poperechny deposit as a function of the depth of drill core sample beneath the surface.

Depth beneath the surface (meters)	Platinum minerals*				PGM solid solutions	PGM sulfides	PGM sulfarsenides
	Pt + Fe	Pt + Fe + Cu	Pt + Fe + Ir	Pt + Fe + Pd			
210–220		+		+			
200–210	+		+	+	+	+	+
190–200		+		+	+		
180–190	+	+	+	+	+	+	+
170–180	+	+	+	+	+	+	+
160–170	+	+	+		+		+

*Platinum minerals are grains of native platinum and platinum-intermetallic compositions with Fe, Cu and Ni (isoferroplatinum, tetraferroplatinum, tulaminite) frequently containing inclusions of other platinum-group minerals.

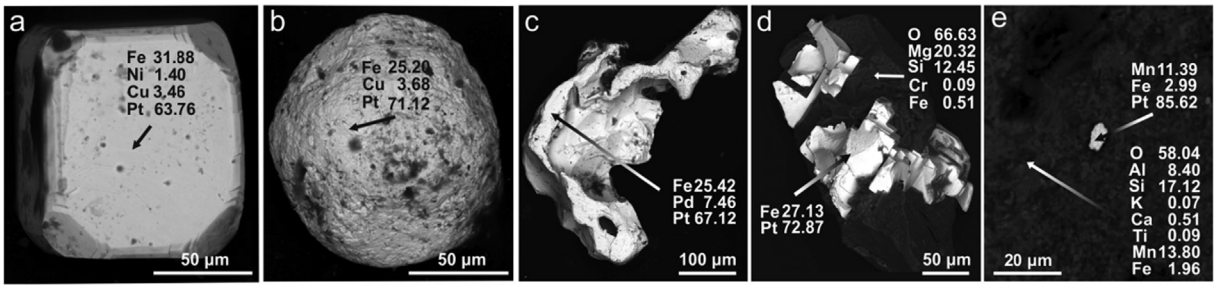

Fig. 3. Scanning electron microscope images of individual Pt-Fe grains from the Poperechny deposit. A–d – Pt-Fe grains from the explosive breccia: a – well-crystallized cubic crystal, b – sub-spherical grain showing surface dissolution; c – irregular grain of Pt-Fe-Pd solid solution; d – intergrowth of a crystal of Pt-Fe solid solution and Mg-olivine. e – platinum micro-particle in the iron-manganese ore. All element contents in this and the following figures are in atomic %.

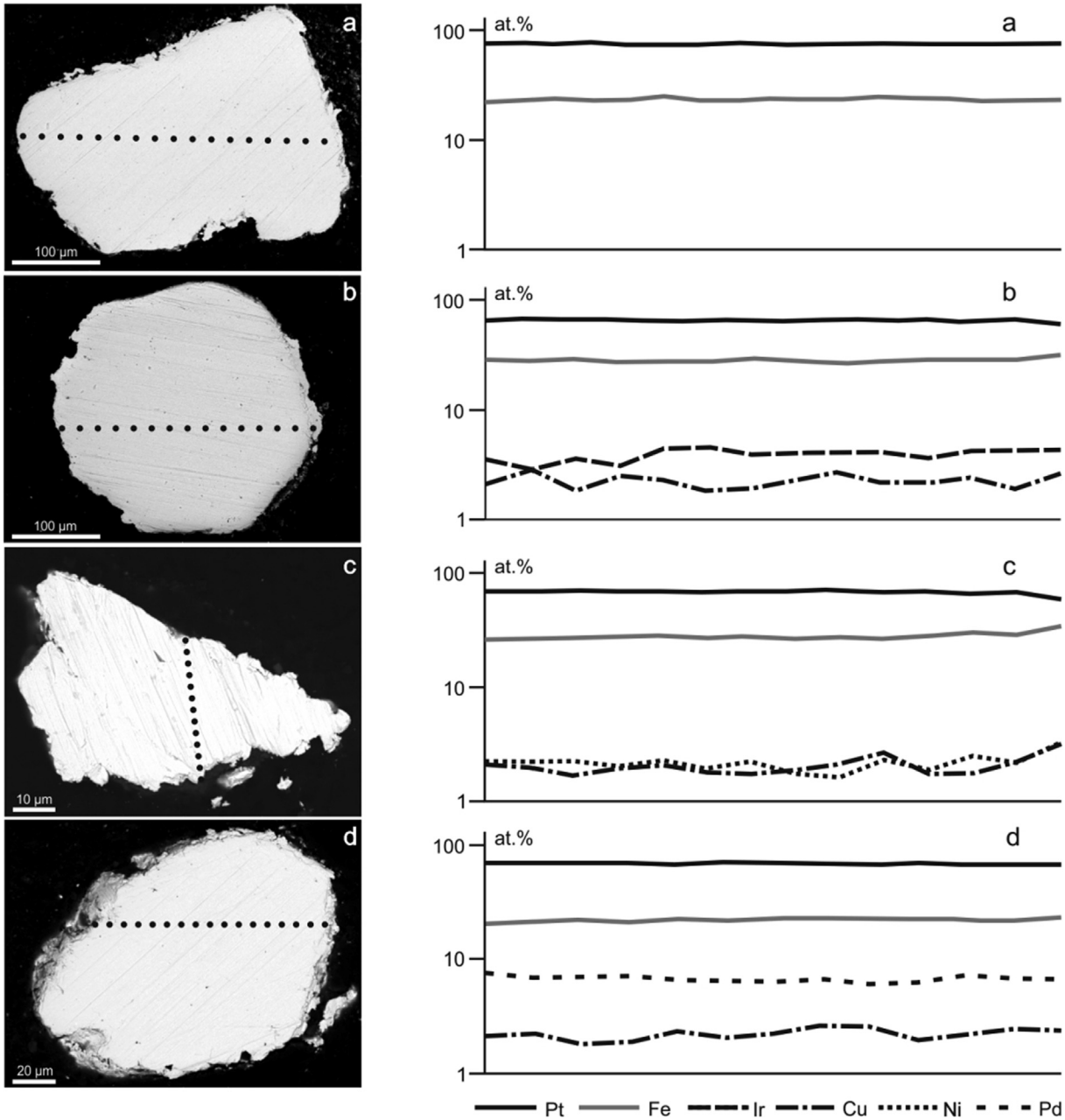

Fig. 4. Microprobe profiles across compositionally homogenous Fe-Pt solid solution grains from the explosive breccia. a – ferroplatinum, b – iridium-bearing ferroplatinum, c – copper-bearing ferroplatinum, d – palladium-bearing ferroplatinum.

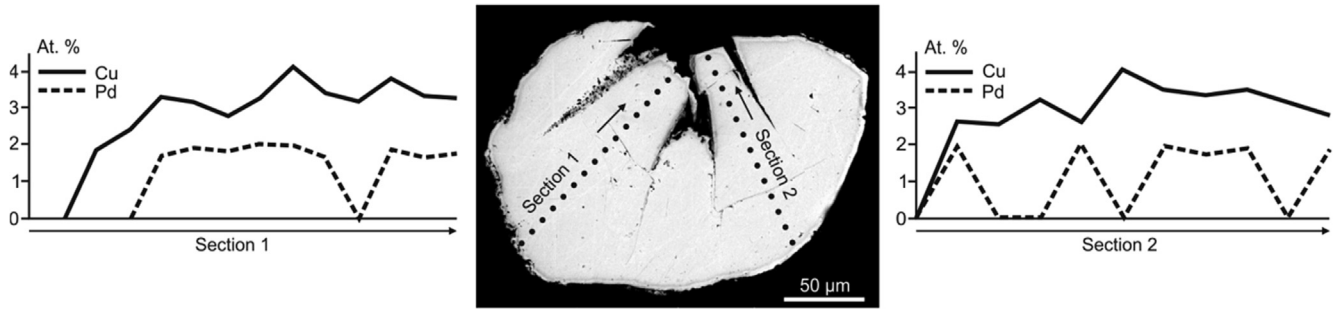

Fig. 5. Variations of copper and palladium content across an individual grain of palladium-bearing Fe-Pt solid solutions from the explosive breccia.

which is typical of sulfarsenides in Ni-Cu-PGE sulfide deposits (Szentpeteri et al., 2002). Rh and Ir sulfides (Fig. 6A–C) occur more frequently than Ru and Os sulfides (Fig. 6A). Both sulfides and sulfarsenides form elongated, needle-like crystals frequently oriented in perpendicular directions (Fig. 6B), as well as larger anhedral to euhedral crystallites (Fig. 6A and D). Some sulfarsenides form euhedral crystals on crystal faces of individual ferroplatinum grains (Fig. 6F).

Ferroplatinum from the explosive breccia frequently contains Ir-enriched PGE solid solutions, which form very fine (first microns in size) anhedral crystals populating platinum grains (Fig. 6A). The average composition of these Ir-rich alloys is as follows (average of 5 grains): Ir = 62.34 at.%, Ru = 12.89 at.%, Rh = 7.02 at.%, Os = 17.76 at.%. One grain of ferroplatinum alloy contains two inclusions of Rh-Pd-arsenides with minor Sb and Ir.

5.2. Iridium-bearing ferroplatinum

Iridium-bearing Fe-Pt solid solutions carry multiple PGE inclusions dominated by Os-rich solid solutions at the expense of Ir-rich solid solutions. Some Fe-Pt grains record reactionary relationships between host iridium-bearing Fe-Pt crystal, Ru-Os-Ir lamellae and later-stage reactionary Os-Ir solid solutions (Fig. 7). Based on textural relationships (Fig. 7), it appears that Ru-Os-Ir lamellae were the crystalline phase in this mineral association. Detailed investigations of their internal structure and chemical variations suggest that these lamellae were probably formed by alternating platinum-group metal compositions with Os contents being negatively correlated with Ru and Ir concentrations (Fig. 7D). Reactionary Os-Ir phase appears to be replacing the Ru-Os-Ir compositions as suggested by relic inclusions of Ru-Os-Ir alloy and textural impregnation of host ferroplatinum crystals by Os-Ir solid solutions (Fig. 7B). Iridium-bearing platinum also contains rare inclusions (total of 6 microinclusions documented) of Ru-Os-Ir sulfides (Ru > Os > Ir) and Ir-sulfarsenides.

5.3. Copper-bearing ferroplatinum

Copper-bearing ferroplatinum frequently contain PGE solid solution inclusions dominated by osmium (Fig. 8). Practically pure osmium inclusions (occasionally with minor iridium) usually form euhedral crystalline platelets (Fig. 8A and B). PGE sulfarsenides (Rh > Ir, Ru) and iridosmine inclusions are observed within rims of several copper-bearing Fe-Pt grains (Fig. 8C and D).

5.4. Palladium-bearing ferroplatinum

This sub-type of ferroplatinum contains inclusions of native osmium (Fig. 9A) and PGE sulfides and sulfarsenides with minor Ni, Cu and Pb (Fig. 9B, D and F). Microprobe analyses of large (50 μm and larger) sulfarsenide grains (Fig. 9F) display increase in Rh and As contents coupled with decrease in Ru and S concentrations from core to rim. Palladium-bearing ferroplatinum frequently displays Pd enrichments towards rims of larger grains (Fig. 9C). In some cases, Pd-bearing

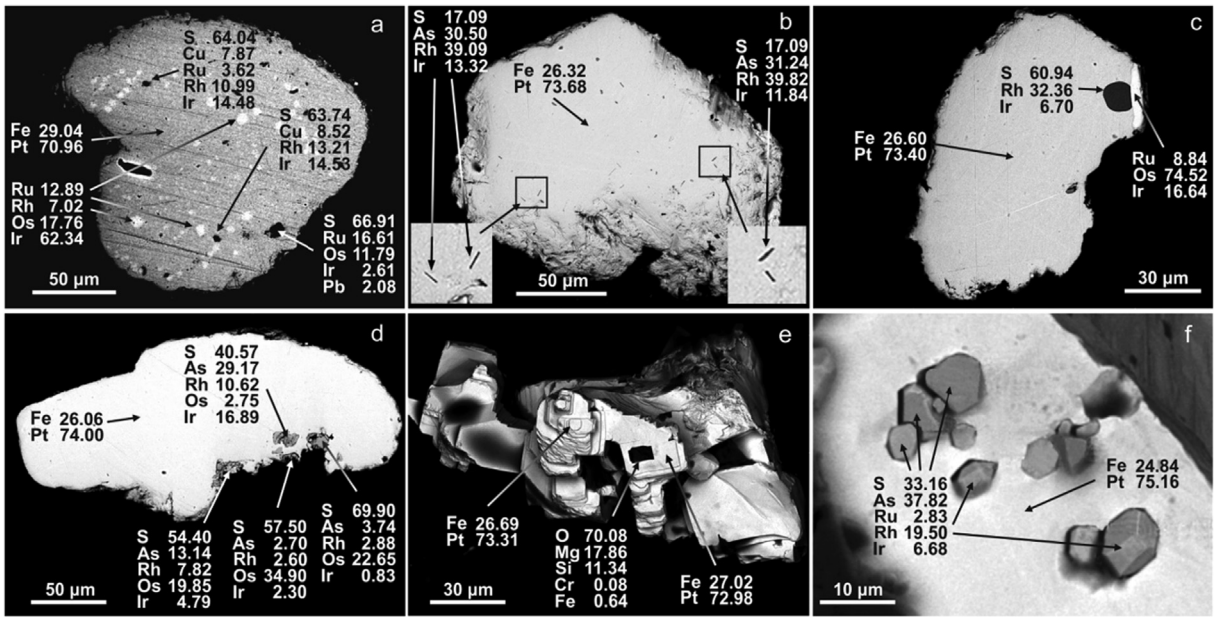

Fig. 6. Inclusions of PGE sulfides (a, c), PGE sulfarsenides (b, d) and PGE solid solutions (a, c) inside individual ferroplatinum crystals and inclusions of forsterite and PGE sulfarsenides (e) on their crystal surfaces.

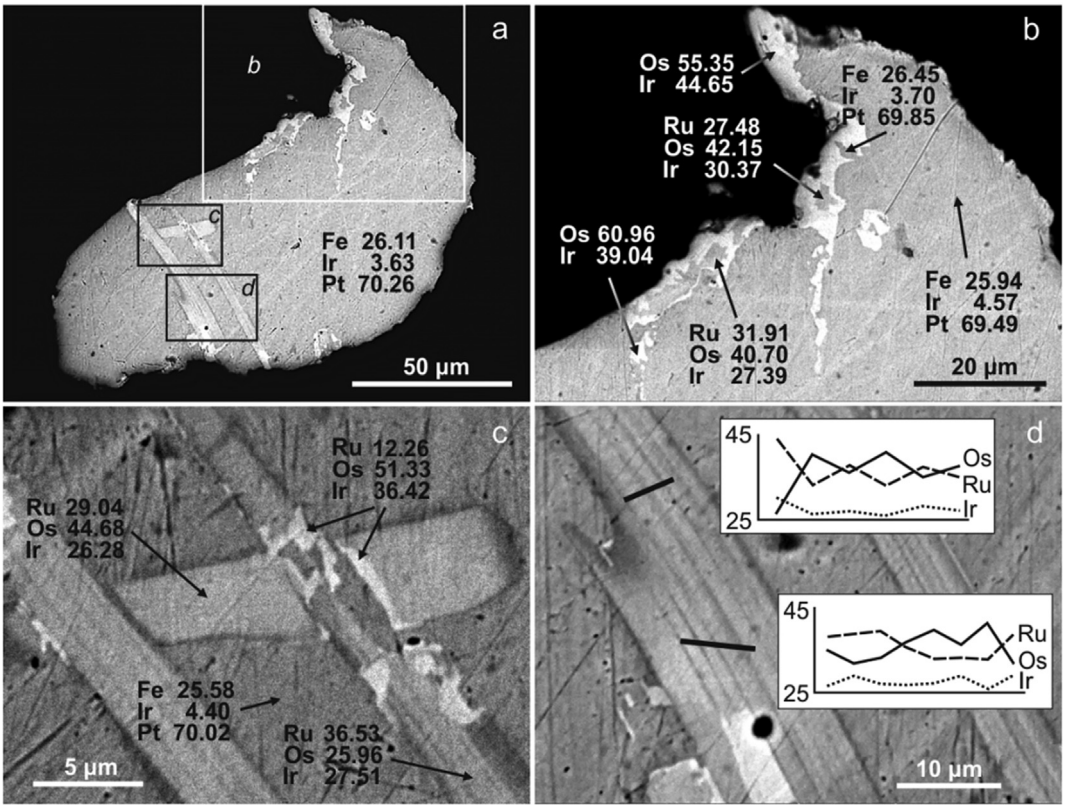

Fig. 7. Inclusions of platinum-group minerals in iridium-bearing ferroplatinum. a – Ru-Os-Ir and Os-Ir solid solution lamellae with enlarged areas presented in b, c and d; b – relics of Ru-Os-Ir alloys in Os-Ir phase; c – development of Os- and Ir-rich phase over Ru-Os-Ir crystals; d – internal structure of Ru-Os-Ir lamellae.

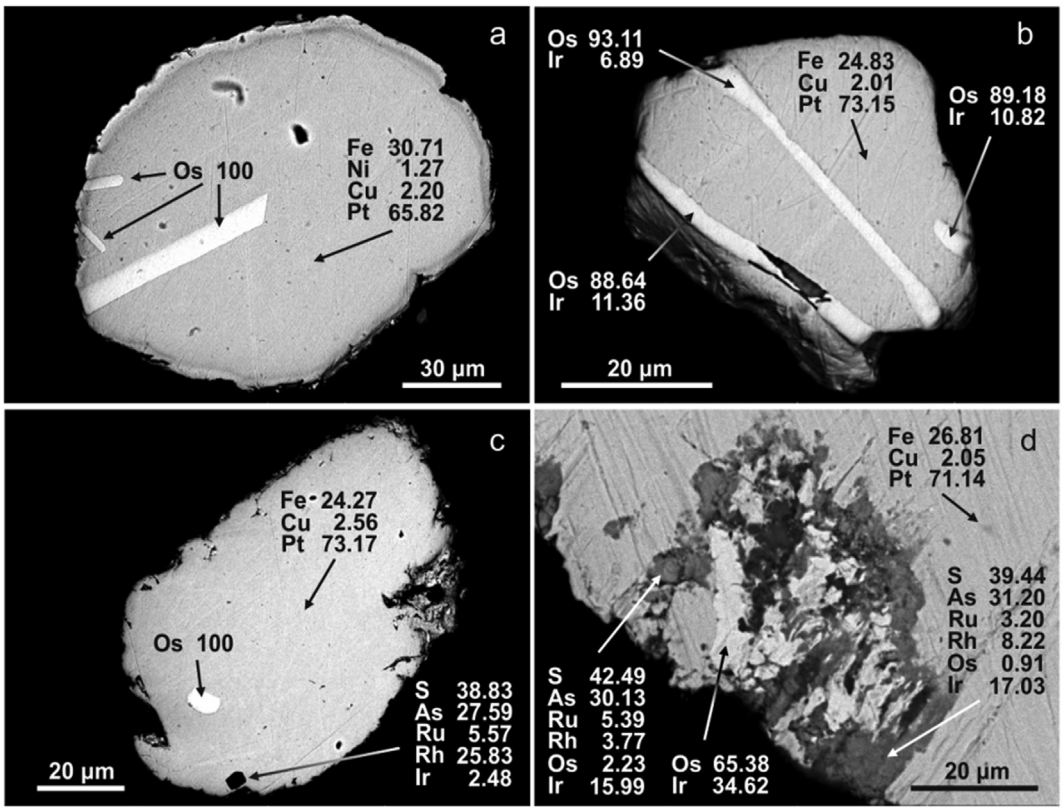

Fig. 8. Inclusions of native osmium (a and b) and PGE sulfarsenides (c and d) in copper-bearing ferroplatinum.

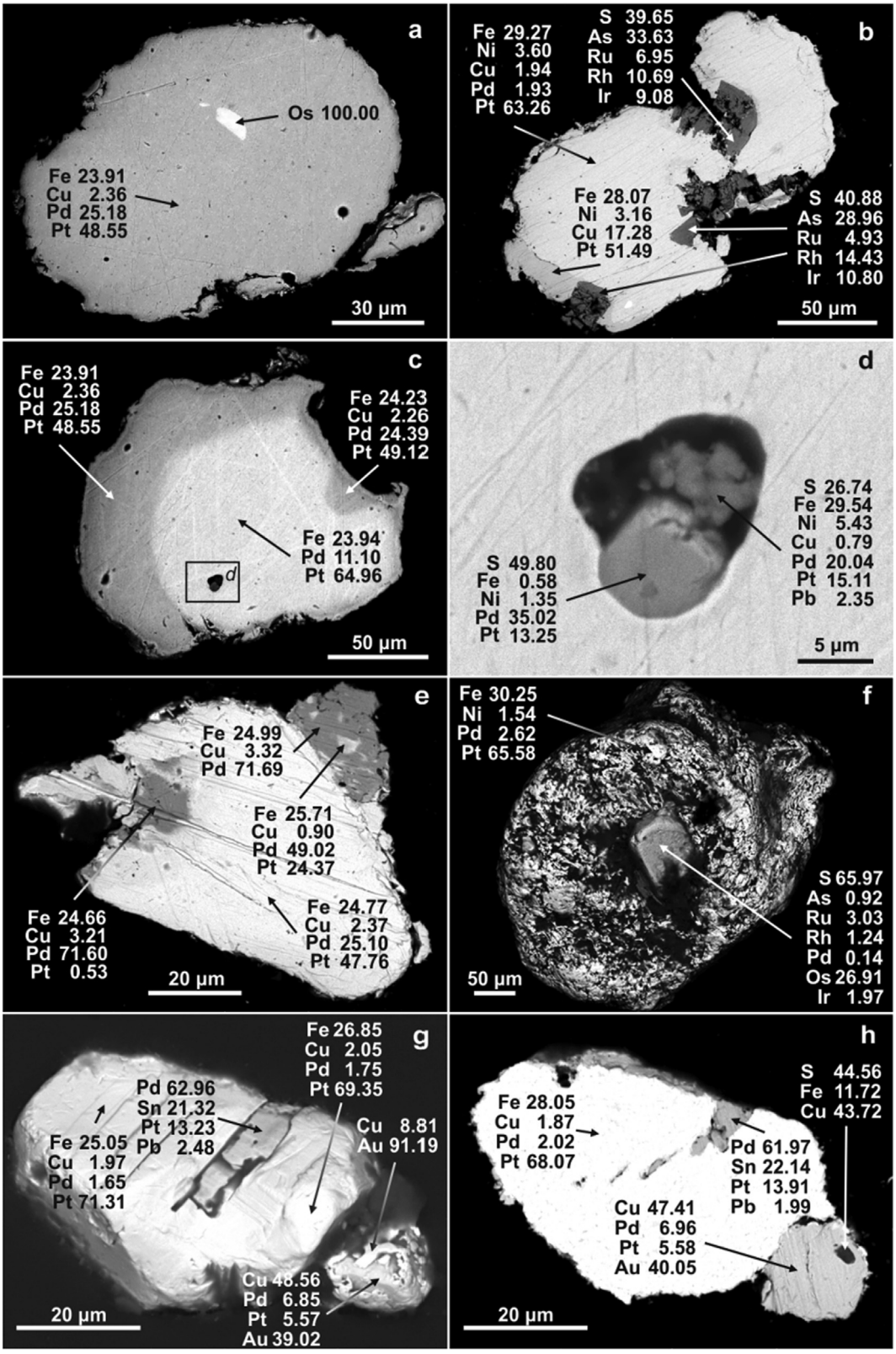

Fig. 9. Inclusions of native osmium (a), palladium (c and e), PGE sulfides and sulfarsenides (b, d and f), palladium plumbostannide and copper-gold solid solutions (g and h) in palladium-bearing ferroplatinum.

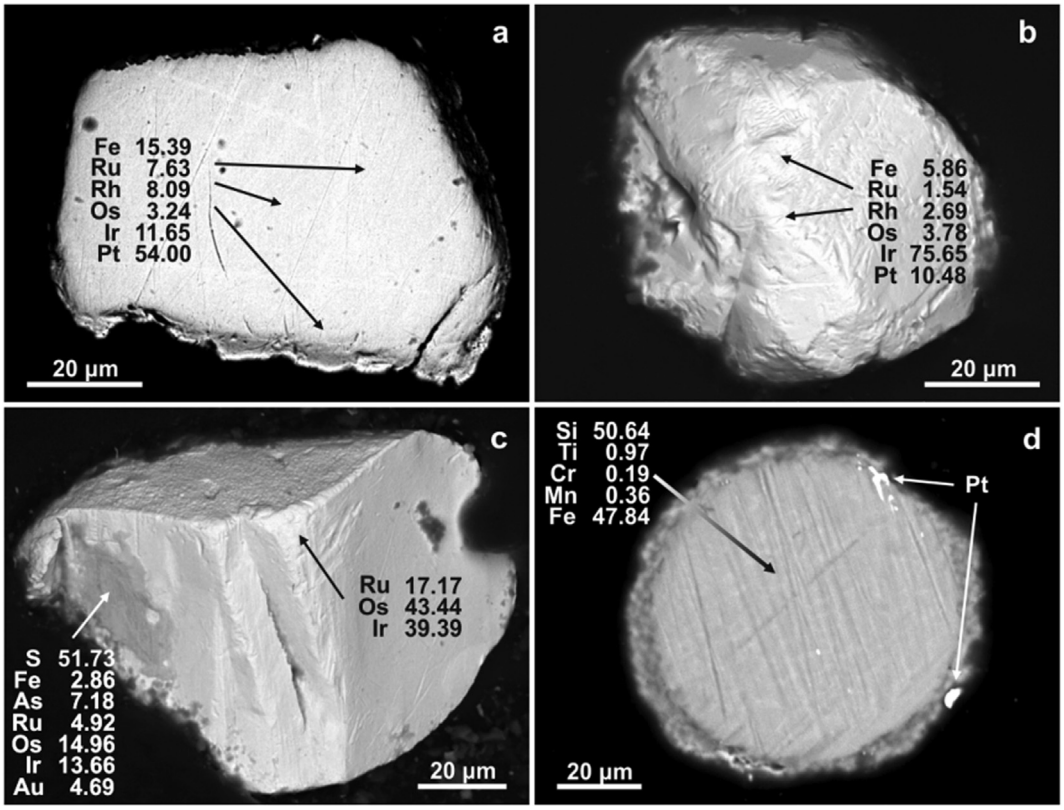

Fig. 10. PGE alloys (A–C) and Fe-Si spherule (D) from the explosive breccia.

ferroplatinum is mantled with palladium rims (Fig. 9E). Other platinum-group minerals observed in palladium-bearing Fe-Pt grains include Pd-Pt-Au-plumbostannide, possibly similar to zvyagentsivite (Cabri and Laflamme, 1997) as well as Pd-Pt-bearing gold-copper alloy rimmed with copper-bearing gold (Fig. 9G and H). A single grain of copper-gold alloy contains an inclusion of chalcopyrite (not shown).

5.5. Other PGE solid solutions

Other PGMs in andesite breccia from the Poperechny iron-manganese deposit are represented by Os-Ru-Rh-Ir-Fe-Pt solid solutions (Fig. 10A), native iridium with minor Pt, Ru, Rh and Os (Fig. 10B), as well as compositionally variable Ru-Ir-Os solid solutions (Fig. 10C). Fig. 10D illustrates rare occurrence of Fe-Si alloy with platinum microparticles, which will be further addressed in the Discussion section.

The latter display rather wide range of compositions (Fig. 11A) comparable with Pt and Pd-free PGE solid solutions in mafic magmas emplaced in continental rifts (Os > Ir > Ru; Hattori and Cabri, 1992; Cabri et al., 1996) and ophiolite chromitites (Os > Ir > Ru and Ru > Os > Ir; Shi et al., 2007; O'Driscoll and Gonzalez-Jimenez, 2016). Some Os-Ir-Ru grains are mantled by PGE-arsenide (Fig. 11C), possibly reflecting increase in sulfur and arsenic activity during differentiation of primary magmatic liquid (Bockrath et al. 2004; Szenpeteri et al., 2002). Based on As-S-PGE relationships in these alloys, sulfides and sulfarsenides presented in Fig. 11A–C, Os-Ru silfides belong to erlichmanite-laurite series with minor Fe (0.45–1.5 atomic % in 80 percent of all studied grains), Ir (0.2–2.8 atomic % in 25 percent of all studied grains) and As (up to 3 atomic %). Three inclusions of PGE alloys contain Pt (0.24–1.59 atomic %). Ir and Rh sulfarsenides are classified as irarsite-hollingworthite with minor Fe (0.2–4.1 atomic %) and Pt (1.48–8.27 atomic %) contents. Two grains of PGE alloys (Fig. 11D) include Os (1.23–1.89 atomic %) and four grains contain Ru

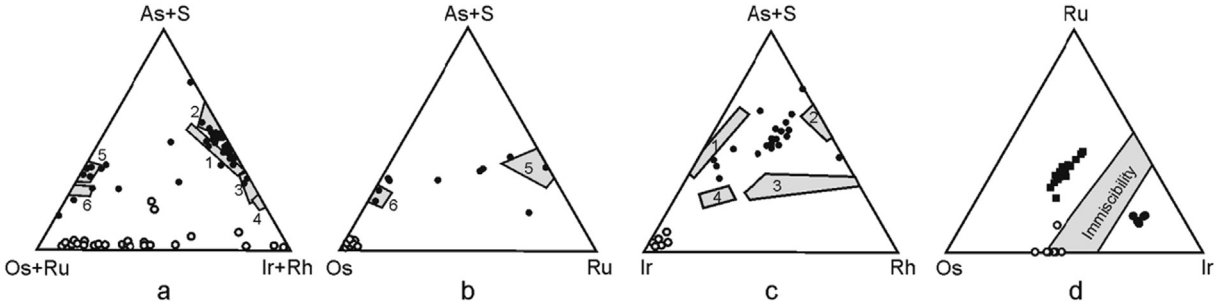

Fig. 11. A–C: Composition of platinum-group minerals (closed circles – sulfides and sulfarsenides, open circles – PGE solid solution series) associated with platinum in the explosive breccia, plotted in As + S – PGE (atomic %) ternary diagrams. Compositional fields for irarsite (1), hollingworthite (2), bowieite (3), kashinite (4), laurite (5) and erlichmanite (6) are modified after Melcher et al. (1997) and Nekrasov et al. (2005). D: Composition of the analyzed PGE solid solutions from the Poperechny breccia in Os-Ru-Ir space, with fields from Harris and Cabri (1991). Note the three compositional groups for Poperechny alloys: low-Ru Os-Ir (open circles), high-Ru (closed squares) and high-Ir (closed circles). Ir-rich alloys contain minor concentrations of rhodium and here are recalculated as Ru + Os + Ir = 100% for the purposes of inter-alloy comparison.

Table 4
Results of ^{190}Pt–^{4}He isotope study of platinum grains in the andesite explosive breccia from the Poperechny Fe-Mn deposit.

Sample	Number of analyzed grains	Weighed sample, milligrams	σ, %	Pt, wt. %	σ, %	^{190}Pt·10^{12}, atoms*	σ%	^{4}He·10^{9}, atoms*	σ%
1	4	0.52	0.4	89.2	0.23	185	0.26	32.8	0.14
2	3	0.377	0.5	89.2	0.22	134.1	0.21	22.4	0.12
3	9	0.753	0.3	88.1	0.25	264.5	0.33	47.1	0.17
4	6	0.519	0.4	88.5	0.26	183.2	0.25	31.2	0.14
5	9	0.601	0.3	86.7	0.28	207.8	0.28	34.4	0.15
6	12	0.55	0.4	88.1	0.24	193.2	0.26	36.1	0.15
7	8	0.516	0.4	88.2	0.25	181.5	0.25	30.3	0.14
8	11	0.462	0.4	88.7	0.27	163.4	0.23	29.8	0.14
9	1	0.236	0.8	88.8	1	83.6	0.15	13.6	0.70
10	1	0.144	1.4	88.8	1	51	0.12	11.3	0.70
11	1	0.114	1.8	88.8	1	40.4	0.11	5.6	0.67
Ta-foil, Cu	–	–	–	–	–	–	–	9.0	0.08

*Amount of isotopes of ^{190}Pt and ^{4}He, extracted from specific weighed sample. Pt content (wt.%) in samples with multiple platinum grains is calculated as average of Pt concentrations in all grains from a particular sample.

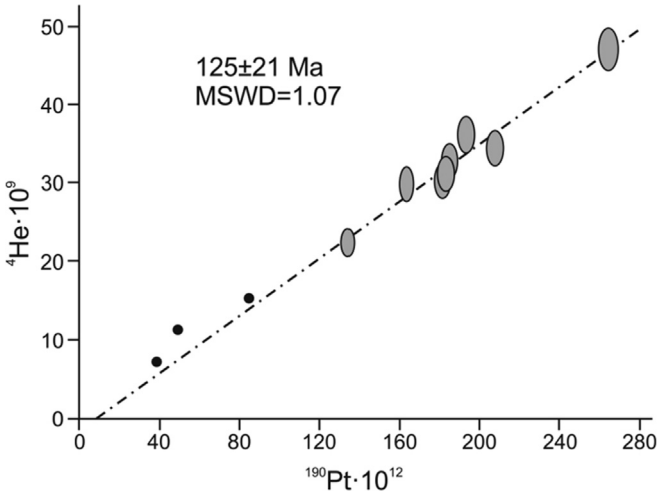

Fig. 12. ^{190}Pt–^{4}He pseudochron for platinum from the explosive breccia based on measurements from eight individual samples following methodology of Shukolyukov et al. (2012, 2014). Data processed using standard Isoplot software (Ludwig, 2003).

(6.14–16.48 atomic %).

5.6. Results of ^{190}Pt and ^{4}He isotope measurements on individual ferroplatinum grains

Concentrations of ^{190}Pt and ^{4}He isotopes were determined for 62 ferroplatinum grains from 8 individual samples of andesite breccia following approaches outlined in (Shukolyukov et al., 2012; Shukolyukov et al., 2014). Details of techniques used in this study are summarized in the section on analytical methods. Results for Poperecnhy samples and runs with pure copper in tantalum foil are listed in Table 4.

A ^{190}Pt-^{4}He pseudochron of 125 Ma ± 21 Ma calculated using standard Isoplot software (Ludwig, 2003) is presented in Fig. 12. In samples 9, 10 and 11 amount of helium is comparable to background values (Table 4). These results were excluded from the isochron calculation and are shown in Fig. 12 as small solid circles strictly for comparative purposes. This pseudochron was not corrected for implanted or ejected helium, which can theoretically adversely affect some isotope-based age determinations (Reiners and Brandon, 2006; Cherniak et al., 2010).

6. Discussion

Andesite explosive breccia associated with the Poperechny iron-manganese deposit carries significant precious metal mineralization (some samples have grades of 11.3 ppm combined PGM and 2.35 ppm Au; Berdnikov et al., 2017) primarily manifested as ferroplatinum along with PGM solid solutions, sulfides and sulfarsenides as well as free gold (Table 2). While PGM behavior in mafic and ultramafic magmas is fairly well documented and understood (Maier and Groves, 2011; O'Driscoll and Gonzalez-Jimenez, 2016), platinum-group minerals in intermediate to felsic rocks are quite rare and conditions of their formation as well as possible sources are poorly constrained at this stage (Setiabudi et al., 2007; Park et al., 2013; Maier et al., 2016). Below we attempt to shed some light on possible origins of platinum-group minerals in evolved igneous associations with some geodynamic inferences in the regional context of accreted terranes of the Russian Far East.

6.1. Evidence for magmatic origin

Textural relationships and compositional variations observed in platinum-group minerals from the explosive andesite breccia suggest two main stages of PGM formation. Ru-Os-Ir solid solutions enriched in Ru (up to 44 atomic %) are found as inclusions in iridium-bearing ferroplatinum grains. Most inclusions of this type are compositionally zoned (alternating Os- and Ru-Ir-enriched zones) possibly reflecting either post-crystallization exsolution textures or compositional variations during magmatic differentiation of parental silicate melt. Ru-Os-Ir alloys from the Poperechny andesite breccia plotted on an Os-Ru-Ir ternary diagram (Fig. 11D) are compositionally similar to PGE alloys crystallized from silicate magma (Brenan and Andrews, 2001; Kamenetsky et al., 2015). Ru-enrichment of some PGM solid solution inclusions in platinum grains is also consistent with mantle origin at high temperatures and pressures (Bird and Bassett, 1980).

Some Ru-Os-Ir crystals are covered with thin rims composed of Ru-poor solid solution with 12.26 at.% Ru, 51.33 at.% Os and 36.42 at.% Ir (Fig. 7). Compositionally similar Os-Ir phase (plotted as open circles in Fig. 11D) also contains fragments of Ru-Os-Ir inclusions and impregnates larger grain of iridum-bearing ferroplatinum (Fig. 7B). The majority of these Ru-free Os-Ir compositions from andesite breccia plot into the immiscibility gap portion of the Os-Ru-Ir ternary diagram (Fig. 11D). Experimental results suggest co-existence of two immiscible phases in this case – Os > 63 at.%, Ir < 37 at.% and Os < 42 at.%, Ir > 58 at.% (Brenan and Andrews, 2001), however neither of these experimentally predicted Os-Ir solid solutions have so far been detected in Poperechny andesite breccia. Products of this immiscibility in the Os-Ru-Ir system might possibly be represented in Poperechny samples by the inclusions of Ir-Ru-Rh-Os alloys in iridium-bearing ferroplatinum crystals (Fig. 6A) plotting to the right of miscibility gap field in the Os-Ir-Ru diagram (Fig. 11D).

Petrographically, earliest PGM assemblages in explosive breccia include Fe-Pt, Os-Ir and Ir-Ru-Rh-Os alloys, which most probably

crystallized from mafic, mantle-derived melt at temperatures of around 1300 (up to 2500 °C for Ru-Os-Ir solid solutions; Bird and Bassett, 1980) to 1050 °C and relatively low sulfur fugacity (O'Driscoll and Gonzalez-Jimenez, 2016; Zaccarini et al., 2018). Similar PGM assemblages of magmatic (cumulate) origin are well documented in the Alaskan-type complexes (Nixon et al., 1990; Tolstykh et al., 2002) and ophiolitic chromitites (Melcher et al., 1997; Ahmed and Arai, 2003; Shi et al., 2007). Further increase in sulfur fugacity accompanied by decrease in temperature during protracted magmatic differentiation of parental magma have led to the formation of erlichmanite-laurite series sulfides and associated sulfarsenides at the expense of PGM solid solutions (Bockrath et al., 2004). This is consistent with observed development of sulfide and sulfarsenide rims on larger ferroplatinum grains (Fig. 6D) and growth of euhedral Ru-Ir-Rh-sulfarsenide crystals on the surfaces of Fe-Pt crystals (Fig. 6F).

Another important feature of PGM mineralization in the explosive breccia associated with the Poperechny Fe-Mn deposit is presence of euhedral inclusions of native osmium in droplet-shaped (magmatic), copper- and iron-bearing platinum (Fig. 8A and C). Native osmium occurs globally as individual micronuggets in PGM placers (Cabri et al., 1996) and is observed as inclusions in Fe-bearing platinum in crustal magma chambers (Melcher et al., 1997; Merkle et al., 2012; Zaccarini et al., 2018). Several authors proposed deep mantle origin (including derivation from the core-mantle boundary region) for osmium-rich alloy assemblages (Bird and Bassett, 1980; Bird et al., 1999), which is consistent with appearance of native osmium and osmium-dominant PGM solid solutions in ultramafic-mafic intrusions associated with deep-seated mantle plumes (Merkle et al. 2012). Alternative explanation suggests precipitation of osmium at rather low temperatures of ~900 °C during cooling-driven unmixing (exsolution) of different Pt-Fe phases and osmium (Zaccarini et al., 2018).

Finally, presence of Si-Fe spherules containing platinum lamellae (Fig. 10D) indicates existence of miscible iron-silica liquid in the parental magmatic system at mantle (at least 1410 °C after Morard et al., 2008) temperatures. Platinum inclusions in Si-Fe spherules suggest that platinum is a near-liquidus phase during proto-magmatic evolution of melts parental to PGM mineralization in Poperechny explosive breccia. This is also consistent with occurrence of platinum in association with Mg-olivine (Fig. 3D), with the latter being, probably together with Cr-spinel, a main liquidus mineral phase during earliest stages of fractionation of mafic parental magma (Kamenetsky et al., 2015).

Secondary-textured precious metal minerals in andesite breccia from the Poperechny deposit include palladium-bearing ferroplatinum solid solutions, palladium stannide and copper-gold solid solutions. Palladium-bearing ferroplatinum frequently forms grains with dissolution surfaces possibly filling spaces between primary rock-forming minerals and is, in turn, replaced by palladium-rich mineral phase. Replacement textures also include growth of palladium stannide as rims on Pd-bearing platinum grains (Fig. 9G and H) and development of gold-enriched rims on copper-gold solid solutions. Since both palladium and gold are highly solvable in both high- and low-temperature oxidized aqueous fluids (Wood et al., 1992; Hanley et al., 2005; Iverson et al., 2019), we interpret these secondary-textured precious metal assemblages as result of hydrothermal processes at crustal depths.

6.2. Possible sources of platinum-group minerals in the explosive breccia

Platinum-group minerals crystallize from mantle-derived mafic and ultramafic magmas in association with forsteritic olivine and Cr-spinel (Roeder and Jamieson, 1992; Finnigan et al., 2008). Os-Ir-Ru and Fe-Pt alloys along with native osmium are documented as chromite-hosted inclusions in a variety of oxidized primary magmas (Kamenetsky et al., 2015). It also appears that, with possible exception of boninites and Mg-andesites (Hamlyn et al., 1985; Peck et al., 1992; Woodland et al., 2002), evolved silicate liquids, such as andesites and dacites, do not precipitate PGMs during the normal course of their magmatic differentiation in the uppermost mantle and crust (Maier et al., 2016). Consequently, platinum-group mineral assemblages in evolved igneous rocks should be treated as xenocrysts acquired from mafic and/or ultramafic lithologies under a range of upper mantle or lower crustal conditions (Park et al., 2013).

Platinum-group mineral assemblage in andesite breccia from the Poperechny iron-manganese deposit is dominated by Fe-bearing platinum, which accounts for 85% of the total number of PGM grains recovered from the explosive breccia drill core (Table 2). This is comparable to percentages of Fe-bearing platinum (> 60%) versus Os-Ir-Ru solid solutions and PGM sulfides and sulfarsenides reported from Ural-Alaskan ultramafic-mafic complexes, especially from the type localities in the Ural Mountains (81% for combined Alaskan-type complexes of Kytlym, Kachkanar, Nizhny Tagil and Uktus; Zaccarini et al., 2018). Another clan of subduction-related, PGM-bearing lithologies, ophiolite cromitites are enriched in Os-Ir-Ru(Rh) alloys, sulfides and arsenides (> 90% in the Urals PGM Province; Zaccarini et al., 2018) as a result of high-temperature crystallization from a hydrous mafic melt under low sulfur fugacity (Ahmed and Arai, 2003; Prichard and Brough, 2009; O'Driscoll and Gonzalez-Jimenez, 2016). The predominance of Pt-Fe alloys over sulfides in the andesite breccia suggests that the crystallization of magmatic PGM assemblages occurred under low sulfur fugacity and gradually increasing oxygen fugacity (mostly due to fractionation of forsteritic olivine). Emergence of a later-stage sulfides and arsenides most probably reflects increase of sulfur fugacity during late magmatic equilibration under slow cooling rate regime (Zaccarini et al., 2018).

The "Alaskan-type" PGM assemblage observed in andesite breccia from the Poperechny deposit may be a result of magma mixing between primary PGM-bearing mafic magmas (such as picrites or ankaramites; Kamenetsky et al., 2015) and subduction-related evolved melts. This is consistent with a clear subduction-related signature (HFSE depletions coupled with LILE and, to a lesser extent, LREE enrichments) observed in the andesite explosive breccia samples. This magma mixing possibly took place in a mid-crustal magma chamber. Progressive increase in fluid pressure in this magmatic reservoir could have triggered an explosive eruption with "mixed" characteristics reflected in the primary magmatic platinum-group mineralization (primitive mafic magma) and presence of the clasts (fragments) with ignimbritic texture (evolved dacitic melt). Alternatively, andesite from the Poperechny deposit could have been derived via protracted crystal fractionation of primary subduction-related picrite or ankaramite magma after formation of dunite core and pyroxenite-gabbro rims, therefore retaining PGM assemblages from genetically related ultramafic-mafic lithologies. Intermediate to felsic rocks (diorites, granodiorites, granites together with andesite porphyry dikes) are well-documented in calc-alkaline plutonic complexes in magmatic arc environments (Snoke et al., 1981; Whalen, 1985; Kepezhinskas et al., 1993).

Finally, observed PGM assemblages could have been scavenged from sub-arc mantle wedge by slab-derived fluids or melts percolating towards the surface (Kepezhinskas et al., 2019). Mantle peridotite xenoliths in volcanic arcs carry platinum-group minerals (Kepezhinskas and Defant, 2001; Miura and Arai, 2014), broadly comparable to the PGM assemblage observed in the Poperechny andesite breccia.

6.3. Implications for regional geodynamics

The isotopic age of 125 ± 21 Ma obtained for Fe-Pt grains from the Poperechny andesite breccia most probably corresponds to a magmatic discharge episode from subduction-related magma conduit broadly comparable in structure and composition to Ural-Alaskan ultramafic-mafic complexes. The latter have been recognized as relatively long-lived, fractionating magma chambers beneath island-arc volcanoes (Conrad and Kay, 1984; DeBari and Coleman, 1989; Kepezhinskas et al., 1993). Mafic diabase dikes intruding carbonates within the eastern portion of the Poperechny deposit are also possible samples of less

evolved melt from the same crustal magma chamber. Unfortunately, no evidence for potential PGM mineralization associated with these diabase dikes exists at this point and all possible comparisons are purely conceptual in nature.

Regional tectonic models based on geologic and seismic tomography data (Zhao et al., 2010; Khanchuk et al., 2016) indicate that the formation of this magmatic plumbing system was possibly related to the opening of slab-window beneath the Lesser Khingan terrane in Early Cretaceous (Zhao et al., 2010). In this scenario, Early Cretaceous slab window was developed within the transform-type continental margin after cessation of Jurassic subduction of Izanagi plate under the composite Tsamusi-Bureya-Khanka super-terrane, previously accreted at the Amur microplate of the Asian continent during Late Jurassic time (Seton et al., 2012; Seton et al., 2015; Ma et al., 2018). Upwelling of astenospheric material through the slab window was probably responsible for the formation of early Cretaceous (100–125 Ma) minor ultramafic-mafic intrusions throughout Eastern Asia in general and Bureinsky block in particular (Khanchuk et al., 2016; Teng et al., 2018). The Izanagi plate subduction also resulted in widespread Cretaceous magmatism gradually migrating in time and space from Mongolia (160–140 Ma) to the Japanese island arc (~80 Ma) (Wang et al., 2006). Poperechny mineralization is located within the northeastern areal of this subduction-related volcanism with most prolific eruptions clustered around 130–120 Ma.

Curiously, some Early Cretaceous volcanics in the Lesser Khingan Range are associated with geochemical anomalies of Co, Ni and Au and also are, at least spatially, coincident with various mineralized systems of Aptian-Albian age hosted in explosive breccia of possible subduction-related genesis (Saksin et al., 2015). This Lower Cretaceous episode of subduction-related PGM petrogenesis can be also possibly correlated with platinum-group metals mineralization in concentrically zoned dunite-alkaline pyroxenite massifs, such as Konder and Chad (Cabri et al., 1998; Nekrasov et al., 2005; Mochalov et al, 2016), which are being interpreted as crustal manifestations of translithospheric thermal diapirs (Burg et al., 2009).

7. Conclusions

Andesite-hosted, platinum-group mineralization associated with the Poperechny iron-manganese deposit (Lesser Khingan Range, Far East Russia) is composed of Fe-Pt solid solutions (85%) and PGM (mostly Os-Ir-Ru) solid solutions, sulfides and sulfarsenides (15%). Fe-Pt solid solutions contain minor Pd, Ir and Cu and contain multiple inclusions of Os-Ir, Ru-Os-Ir and Ir-rich solid solutions along with rare grains of euhedral osmium. Pt-Fe and Os-Ir-Ru solid solutions were formed during high-temperature fractionation of mantle-derived mafic parental melt. Magmatic sulfides mostly belong to the erlichmanite-laurite series, while Pd-Pt plumbostannide and copper-gold solid solutions reflect late magmatic re-crystallization and post-magmatic hydrothermal metasomatism. PGM-bearing andesite breccia was most probably formed during magma mixing (between mafic and felsic end-members) and discrete discharge of intermediate silicate magma from crustal magma reservoir. Early Cretaceous (~125 Ma) age of platinum in andesite breccia suggests that such reservoir (compositionally similar to Ural-Alaskan type complexes) could have been formed during Late Mesozoic subduction of Izanagi plate along the southern margin of North Asian continent.

Acknowledgements

Comments by Dr. Zhang Zhaochong and an anonymous reviewer on the earlier version of this paper and editorial handling of the manuscript by Dr. Zhang Zhaochong are greatly appreciated. This work was carried out within the State Assignment for the Institute of Tectonics and Geophysics, FEB RAS, Khabarovsk, Russian Federation. We thank L.M. Ilyina (XRF), A.V. Shtareva (ICP-MS) and V.O.Krutikova (SEM-EDS) for their help in analytical investigations at the KhIAC and colleagues at the MI FEB RAS for separation of noble metals from andesite breccia samples.

Declarations of Competing Interest

None.

Appendix A. Supplementary data

Supplementary data to this article can be found online at https://doi.org/10.1016/j.oregeorev.2020.103352.

References

Ahmed, A.H., Arai, S., 2003. Platinum-group minerals in podiform chromitites of the Oman ophiolite. Can. Mineral. 41, 597–616.
Barnes, S.-J., Mungall, J.E., Maier, W.D., 2015. Platinum group elements in mantle melts and mantle samples. Lithos 232, 395–417.
Berdnikov, N.V., Nevstruev, V.G., Saksin, B.G., 2017. Genetic aspects of the noble metal mineralization at the Poperechnoe deposit, lesser Khingan, Russia. Russ. J. Pacific Geol. 11, 421–435.
Bird, J.M., Bassett, W.A., 1980. Evidence of a deep mantle history in terrestrial osmium-iridium-ruthenium alloys. J. Geophys. Res. 85, 5461–5470.
Bird, J.M., Meibom, A., Frei, R., Nagler, T.F., 1999. Osmium and lead isotopes of rare OsIrRu minerals: derivation from the core-mantle boundary region? Earth Planet. Sci. Lett. 170, 83–92.
Bockrath, C., Ballhaus, C., Holzheid, A., 2004. Stabilities of laurite RuS_2 and monosulphide liquid solution at magmatic temperature. Chem. Geol. 2008, 265–271.
Bowles, J.F.W., 1990. Platinum-iron alloys, their structure and magnetic characteristics in relation to hydrothermal and low-temperature genesis. Mineral. Petrol. 43, 37–47.
Brenan, J.M., Andrews, D., 2001. High-temperature stability of laurite and Ru-Os-Ir alloy and their role in PGE fractionation in mafic magmas. Can. Mineral. 39, 341–360.
Burg, J.-P., Bodinier, J.-L., Gerya, T., Bedini, R.-M., Boudier, F., Dautria, J.-M., Prikhodko, V.S., Efimov, A., Pupier, E., Balanec, J.-L., 2009. Translithospheric mantle diapirism: geological evidence and numerical modeling of the Kondyor zoned ultramafic complex (Russian Far East). J. Petrol. 50, 289–321.
Cabri, L.J., Feather, M., 1975. Platinum-iron alloys: a nomenclature based on a study of natural and synthetic alloys. Can. Mineral. 13, 117–126.
Cabri, L.J., Laflamme, J.H.G., 1997. Platinum-group minerals from the Konder massif, Russian Far East. Mineral. Rec. 28, 97–106.
Cabri, L.J., Harris, D.C., Weiser, T.W., 1996. Mineralogy and distribution of platinum-group mineral (PGM) placer deposits of the world. Explor. Min. Geol. 5, 73–167.
Cabri, L.J., Stern, R.A. and Czamanske, G.K., 1998. Osmium isotope measurements of Pt-Fe alloy placer nuggets from the Konder intrusion using a SHRIMP II ion microprobe. Pp. 55–58 in: Abstracts of the 8th International Platinum Symposium, 28 June – 3 July 1998, The South African Institute of Mining and Metallurgy, Johannesburg 1998, Symp. Series S18.
Cherniak, D.J., Hervig, R., Koepke, J., Zhang, Y., Zhao, D., 2010. Analytical methods in diffusion studies. Rev. Mineral. Geochem. 72, 107–169.
Conrad, W.K., Kay, R.W., 1984. Ultramafic and mafic inclusions from Adak Island: crystallization history, and implications for the nature of primary magmas and crustal evolution in the Aleutian arc. J. Petrol. 25, 88–125.
DeBari, S.M., Coleman, R.G., 1989. Examination of the deep levels of an island arc: evidence from the Tonsina ultramafic-mafic assemblage, Tonsina, Alaska. J. Geophys. Res. 94, 4373–4391.
Didenko, A.N., Kaplin, V.B., Malyshev, Yu.F., Shevchenko, B.F., 2010. Lithospheric structure and Mesozoic geodynamics of the eastern Central Asian orogen. Russ. Geol. Geophys. 51, 492–506.
Finnigan, C.S., Brenan, J.M., Mungall, J.E., McDonough, W.F., 2008. Experiments and models bearing on the role of chromite as a collector of platinum group minerals by local reduction. J. Petrol. 49, 1647–1665.
Hamlyn, P.R., Keays, R.R., Cameron, W.E., Crawford, A.J., Waldron, H.M., 1985. Precious metals in magnesian low-Ti lavas: implications for metallogenesis and sulfur saturation in primary magmas. Geochim. Cosmochim. Acta 49, 1797–1811.
Hanley, J.J., Mungall, J.E., Pettke, T., Spooner, E.T.C., Bray, C.J., 2005. Ore metal redistribution by hydrocarbon-brine and hydrocarbon-halide melt phases, North Range footwall of the Sudbury Igneous Complex, Ontario, Canada. Min. Deposita 40, 237–256.
Hattori, K., Cabri, J.L., 1992. Origin of platinum-group-mineral nuggets inferred from an osmium-isotope study. Can. Mineral. 30, 289–301.
Hawkesworth, C.J., Gallagher, K., Hergt, J.M., McDermott, F., 1993. Mantle and slab contributions in arc magmas. Annu. Rev. Earth Planet. Sci. 21, 175–204.
Iverson, A.A., Webster, J.D., Rowe, M.C., Neill, O.K., 2019. Fluid-melt trace-element partitioning behavior between evolved melts and aqueous fluids: experimental constraints on the magmatic-hydrothermal transport of metals. Chem. Geol. 516, 18–41.
Kamenetsky, V.S., Park, J.-W., Mungall, J.E., Pushkarev, E.V., Ivanov, A.V., Kamenetsky, M.B., Yaxley, G.M., 2015. Crystallization of platinum-group minerals from silicate melts: evidence from Cr-spinel-hosted inclusions in volcanic rocks. Geology 43, 903–906.
Kepezhinskas, P.K., Defant, M.J., 2001. Nonchondritic Pt/Pd ratios in arc mantle

xenoliths: evidence for platinum enrichment in depleted island-arc mantle sources. Geology 29, 851–854.
Kepezhinskas, P.K., Reuber, I., Tanaka, H., Miyashita, S., 1993. Zoned calc-alkaline plutons in Northeastern Kamchatka, Russia: implications for the crustal growth in magmatic arcs. Mineral. Petrol. 49, 147–174.
Kepezhinskas, P., Kepezhinskas, N., Berdnikov, N., 2019. Gold, platinum and palladium enrichments in arcs: role of mantle wedge, arc crust and halogen-rich slab fluids. E3S Web of Conferences 98, 08010. doi:10.1051/e3sconf/20199808010.
Kepezhinskas, N., Kamenov, G.D., Foster, D.A., Kepezhinskas, P., 2020... Petrology and geochemistry of alkaline basalts and gabbroic xenoliths from Utila island (Bay Islands, Honduras): insights into back-arc processes in the Central American Volcanic Arc. Lithos 352–353, 105306.
Khanchuk, A.I., Nevstruev, V.G., Berdnikov, N.V., Nechaev, V.P., 2013. Petrochemical characteristics of carbonaceous shales in the eastern Bureya massif and their precious metal mineralization. Russ. Geol. Geophys. 54, 627–636.
Khanchuk, A.I., Didenko, A.N., Popeko, L.I., Sorokin A.A., Shevchenko, B.F., 2015. Structure and evolution of the Mongol-Okhotsk orogenic belt. In: The Central Asian Orogenic Belt: Geology, Evolution, Tectonics, and Models. A. Kröner (Ed.). Borntraeger Science Publishers, Stüttgart, pp. 211–234.
Khanchuk, A.I., Kemkin, I.V., Kruk, N.N., 2016. The Sikhote-Alin orogenic belt, Russian South East: terranes and the formation of continental lithosphere based on geological and isotopic data. J. Asian Earth Sci. 120, 117–138.
Lambert, D.D., Morgan, J.W., Walker, R.J., Shirey, S.B., Carlson, R.W., Zientek, M.L., Koski, M.S., 1989. Rhenium-osmium and samarium-neodymium isotopic systematics of the Stillwater Complex. Science 244, 1169–1174.
Liu, K., Zhang, J., Wilde, S.A., Lin, Sh., Guo, F., Kasatkin, S.A., Golozoubov, V.V., Ge, M., Wang, M., Wang, J., 2017. U-Pb dating and Lu-Hf isotopes of detrital zircons from the Southern Sikhote-Alin Orogenic Belt, Russian Far East: tectonic implications for the Early Cretaceous evolution of the Northwest Pacific margin. Tectonics 36, 2555–2598.
Luan, J.P., Wang, F., Xu, W.L., Ge, W.C., Sorokin, A.A., Wang, Z.W., Guo, P., 2017. Provenance, age, and tectonic implications of Neoproterozoic strata in the Jiamusi Massif: evidence from U-Pb ages and Hf isotope compositions of detrital and magmatic zircons. Precambr. Res. 297, 19–32.
Ludwig, K.R., 2003. User's manual for Isoplot 3.00: a geochronological toolkit for Microsoft Excel. Berkeley Geochronol. Center Spec. Publ. 4, 25–32.
Ma, J., Tian, Y., Lin, C., Zhao, D., Feng, X., Zhu, H., 2018. P-wave tomography of Northeast Asia: constraints on the western Pacific plate subduction and mantle dynamics. Phys. Earth Planet. Inter. 274, 105–126.
Maier, W.D., 2005. Platinum-group element (PGE) deposits and occurrences: mineralization styles, genetic concepts and exploration data. J. Afr. Earth Sci. 41, 165–191.
Maier, W.D., Groves, D.I., 2011. Temporal and spatial controls on the formation of magmatic PGE and Ni-Cu deposits. Miner. Deposita 46, 841–857.
Maier, W.D., Barnes, S.J., Karykowski, B.T., 2016. A chilled margin of komatiite and Mg-rich basaltic andesite in the western Bushveld Complex, South Africa. Contrib. Miner. Petrol. 171, 57–79.
Malitch, K.N., Thalhammer, O.A.R., 2002. Pt-Fe nuggets derived from clinopyroxenite-dunite massifs, Russia: a structural, compositional and osmium-isotope study. Can. Mineral. 40, 395–418.
Malitch, K.N., Efimov, A.A., Badanina, I.Yu., 2012. The age of Kondyor massif dunites, Aldan Province, Russia: first U-Pb isotopic data. Dokl. Earth Sci. 446, 1054–1058.
Melcher, F., Grum, W., Simon, G., Thalhammer, T.V., Stumpfl, E.F., 1997. Petrogenesis of the ophiolitic giant chromite deposits of Kempersai, Kazakhstan: a study of solid and fluid inclusions in chromite. J. Petrol. 38, 1419–1458.
Merkle, R.K.W., Malitch, K.N., Graser, P.P.H., Badanina, I.Yu., 2012. Native osmium from the Guli Massif, Northern Siberia, Russia. Mineral. Petrol. 104, 115–127.
Miura, M., Arai, S., 2014. Platinum-group element and mineral characteristics of sub-arc chromitite xenoliths from the Takashima alkali basalt, Southwest Japan arc. Can. Mineral. 52, 899–916.
Mochalov, A.G., Yakubovich, O., Bortnikov, N.P., 2016. ^{190}Pt-^{4}He age of PGE ores in the alkaline-ultramafic Kondyor massif (Khabarovsk district, Russia). Dokl. Earth Sci. 469, 846–850.
Mochalov, A.G., Yakubovich, O., Zolotarev, A.A., 2018. Structural transformation and retention of radiogenic ^{4}He in platinum minerals under mechanical deformations. Dokl. Earth Sci. 480, 591–594.
Morard, G., Sanloup, C., Guillot, B., Fiquet, G., Mezouar, M., Perrillat, J.P., Garbarino, G., Mibe, K., Komabayashi, T., Funakoshi, K., 2008. In situ structural investigation of Fe-S-Si immiscible liquid system and evolution of Fe-S bond properties with pressure. J. Geophys. Res. 113, B10205. doi:10.1029/2008JB005663.
Moroni, M., Girardi, V.A.V., Ferrario, A., 2001. The Serra Pelada Au-PGE deposit, Sierra dos Carajas (Pará State, Brazil): geological and geochemical indications for a composite mineralizing process. Miner. Deposita 36, 768–785.
Naldrett, A.J., Wilson, A., Kinnaird, J., Chunnett, G., 2009. PGE tenor and metal ratios within and below the Merensky Reef, Bushveld Complex: implications for its genesis. J. Petrol. 50, 625–659.
Nekrasov, I.Ya., Lennikov, A.M., Zalishchak, B.L., Oktyabrsky, R.A., Ivanov, V.V., Sapin, V.I., Taskaev, V.I., 2005. Compositional variations in platinum-group minerals and gold, Konder alkaline-ultrabasic massif, Aldan Shield, Russia. Can. Mineral. 43, 637–654.
Nevstruyev, V.G., Berdnikov, N.V., Didenko, A.N., Saksin, B.G., Lavrik, N.A., 2018. Fluidolites as a source of primary gold-platinum mineralization in the Poperechnoe deposit (Malyi Khingan Range, Russia). Dokl. Earth Sci. 482, 1203–1206.
Nixon, G.T., Cabri, L.J., Laflamme, J.H.G., 1990. Platinum-group-element mineralization in lode and placer deposits associated with the Tulameen Alaskan-type complex, British Columbia. Can. Mineral. 28, 503–535.
O'Driscoll, B., Gonzalez-Jimenez, J.M., 2016. Petrogenesis of the platinum-group minerals. Rev. Mineral. Geochem. 81, 489–578.
Park, J.-W., Campbell, I., Arculus, R., 2013. Platinum-alloy and sulfur saturation in an arc-related basalt to rhyolitic suite: evidence from the Pual Ridge lavas, the Eastern Manus Basin. Geochim. Cosmochim. Acta 101, 76–95.
Peck, D.C., Keays, R.R., Ford, R., 1992. Direct crystallization of refractory platinum-group element alloys from boninitic magmas: evidence from western Tasmania. Aust. J. Earth Sci. 39, 373–387.
Pentek, A., Molnar, F., Tuba, G., Watkinson, D.H., Jones, P.C., 2013. The significance of partial melting processes in hydrothermal low sulfide Cu-Ni-PGE mineralization within the footwall of the Sudbury igneous complex, Ontario, Canada. Econ. Geol. 108, 59–78.
Perfit, M.R., Gust, D.A., Bence, A.E., Arculus, R.J., Taylor, S.R., 1980. Chemical characteristics of island-arc basalts: implications for mantle sources. Chem. Geol. 30, 227–256.
Prichard, H.M., Brough, C., 2009. Potential of ophiolite complexes to host PGE deposits. In: New Developments in Magmatic Ni-Cu and PGE Deposits. Li, C., Ripley, E.M. (Eds). Geological Publishing House, Beijing, China. pp. 277–290.
Reiners, P.W., Brandon, M.T., 2006. Using thermochronology to understand orogenic erosion. Annu. Rev. Earth Planet. Sci. 34, 419–466.
Roeder, P.L., Jamieson, H.E., 1992. Composition of chromite and co-existing Pt-Fe alloy at magmatic temperatures. Aust. J. Earth Sci. 39, 419–426.
Saksin, B.G., Nevstruev, V.G., Usikov, V.I., 2015. Current state of the art of exploration of endogenic deposits of noble metals in the Lesser Khingan Range in the Far East of Russia. Russ. J. Pacific Geol. 9, 57–63.
Sato, H., 1977. Nickel content of basaltic magmas: identification of primary magmas and a measure of the degree of olivine fractionation. Lithos 10, 113–120.
Savatenkov, V.M., Mochalov, A.G., 2013. Age and sources of dunites of Konder Massif (Aldan Shield). Dokl. Earth Sci. 482, 1331–1335.
Setiabudi, B.T., Campbell, I.H., Martin, C.E., Allen, C.M., 2007. Platinum group element geochemistry of andesite intrusions of the Kelian region, East Kalimantan, Indonesia: implications of gold depletion in the intrusions associated with the Kelian gold deposit. Econ. Geol. 102, 95–108.
Shi, R., Alard, O., Zhi, X., O'Reilly, S.Y., Pearson, N.J., Griffin, W.L., Zhang, M., Chen, X., 2007. Multiple events in the Neo-Tethyan oceanic upper mantle: evidence from Ru-Os-Ir alloys in the Luobusa and Dongqiao ophiolitic podiform chromitites. Tibet. Earth Planet. Sci. Lett. 261, 33–48.
Sener, A.K., Grainger, C.J., Groves, D.I., 2002. Epigenetic gold-platinum-group element deposits: examples from Brazil and Australia. Appl. Earth Sci. 111, 65–73.
Seton, M., Müller, R.D., Zahirovic, S., Gaina, C., Torsvik, T., Shepard, G., Talsma, A., Gurnist, M., Turner, M., Maus, S., Chandler, M., 2012. Earth Sci. Rev. 113, 212–270.
Seton, M., Flament, N., Whittaker, J., Müller, R.D., Gurnis, M., Bower, D.J., 2015. Ridge subduction sparked reorganization of the Pacific plate-mantle system 60–50 million years ago. Geophys. Res. Lett. 42, 1–9.
Shukolyukov, Yu.A., Yakubovich, O.V., Mochalov, A.G., Kotov, A.B., Sal'nikova, E.B., Yakovleva, A.Z., Korneev, S.I., Gorokhovskii, B.M., 2012. New geochronometer for the direct isotopic dating of native platinum minerals (190Pt-4He method). Petrology 20, 491–505.
Shukolyukov, Yu.A., Yakubovich, O.V., Mochalov, A.G., 2014. Dating platinum mineralization by the novel 190Pt-4He method of isotope geochronology. In: 12th International Platinum Symposium, Yekaterinburg, Russia, IGG UB RAS. pp. 218–220.
Smirnova, Yu.N., Sorokin, A.A., Kotov, A.B., Kovach, V.P., 2016. Tectonic conditions of sedimentation and source areas of Upper Proterozoic and Lower Paleozoic terrigeneous deposits of the Lesser Khingan Terrane of the Central Asian Fold Belt. Stratigr. Geol. Correlation 24, 219–241.
Snoke, A.W., Quick, J.E., Bowman, H.R., 1981. Bear Mountain igneous complex, Klamath Mountains, California: an ultrabasic to silicic calc-alkaline suite. J. Petrol. 22, 501–552.
Sorokin, A.A., Kotov, A.B., Salnikova, E.B., Sorokin, A.P., Yakovleva, S.Z., Fedoseenko, A.M., Plotkina, Yu.V., 2010. First data on the age of Early Paleozoic granitoids from the Malyi Khingan Terrane of the Central Asian Fold Belt. Dokl. Earth Sci. 431, 299–303.
Szenpeteri, K., Watkinson, D.H., Molnar, F., Jones, P.C., 2002. Platinum-group elements-Co-Ni-Fe sulfarsenides and mineral paragenesis in Cu-Ni-platinum-group element deposits, Copper Cliff North area, Sudbury, Canada. Econ. Geol. 97, 1459–1470.
Teng, X.-M., Santosh, M., Tang, L., 2018. The Early Cretaceous Shangzhuang layered mafic intrusion and its bearing on decratonization of the North China Craton. Geol. Mag. 155, 1475–1506.
Thirlwall, M.F., Smith, T.E., Graham, A.M., Theodorou, N., Hollings, P., Davidson, J.P., Arculus, R.J., 1994. High field strength element anomalies in arc lavas: source or process? J. Petrol. 35, 819–838.
Tolstykh, N.D., Foley, J.Y., Sidorov, E.G., Laajoki, K.V.O., 2002. Composition of the platinum-group minerals in the Salmon River placer deposit, Goodnews Bay, Alaska. Can. Mineral. 40, 463–471.
Walker, R.J., Brandon, A.D., Bird, J.M., Piccoli, P.M., McDonough, W.F., Ash, R.D., 2005. ^{187}Os-^{186}Os systematics of Os-Ir-Ru alloy grains from southwestern Oregon. Earth Planet. Sci. Lett. 230, 211–226.
Wang, F., Zhou, X., Zhang, L., Ying, J., Zhang, Y., Wu, F., Zhu, R., 2006. Late Mesozoic volcanism in the Great Xing'an Range (NE China): timing and implications for the dynamic setting of NE Asia. Earth Planet. Sci. Lett. 251, 170–198.
Whalen, J.B., 1985. Geochemistry of an island-arc plutonic suite: the Uasilau-Yau Yau intrusive complex, New Britain, P.N.G. J. Petrol. 26, 603–632.
Wood, B.J., Turner, S.P., 2009. Origin of primitive high-Mg andesite: constraints from natural examples and experiments. Earth Planet. Sci. Lett. 283, 59–66.
Wood, S.A., Mountain, B.W., Pan, P., 1992. The aqueous geochemistry of platinum, palladium and gold: recent experimental constraints and a re-evaluation of

theoretical predictions. Can. Mineral. 30, 955–982.
Woodhead, J., Eggins, S., Gamble, J., 1993. High field strength and transition element systematics in island arc and back-arc basin basalts: evidence for multi-phase melt extraction and a depleted mantle wedge. Earth Planet. Sci. Lett. 114, 491–504.
Woodland, S.J., Pearson, D.G., Thirlwall, M.F., 2002. A platinum group element and Re-Os isotope investigation of siderophile element recycling in subduction zones: comparison of Grenada, Lesser Antilles Arc, and the Izu-Bonin Arc. J. Petrol. 43, 171–198.
Yang, H., Ge, W., Zhao, G., Dong, Y., Bi, J., Wang, Zh., Yu, J., Zhang, Y., 2014. Geochronology and geochemistry of Late Pan-African intrusive rocks in the Jiamusi-Khanka Block, NE China: petrogenesis and geodynamic implications. Lithos 208–209, 220–236.
Yao, Zh., Qin, K., Mungall, J.E., 2018. Tectonic controls on Ni and Cu contents of primary mantle-derived magmas for the formation of magmatic sulfide deposits. Am. Mineral. 103, 1545–1567.
Zaccarini, F., Garuti, G., Pushkarev, E., Thalhammer, O., 2018. Origin of platinum-group minerals (PGM) inclusions in chromite deposits of the Urals. Minerals 8, 379. https://doi.org/10.3390/min8090379.
Zhao, D., Pirajno, F., Dobretsov, N.L., Liu, L., 2010. Mantle structure and dynamics under East Russia and adjacent regions. Russ. Geol. Geophys. 51, 925–938.